REVERSING FLOW IN MICROCHANNEL EVAPORATORS

Hrnjak P.* and Tuo H.
*Author for correspondence
Department of Mechanical Science and Engineering,
University of Illinois at Urbana-Champaign,
Urbana, IL, USA
CTS, 2209 Willow Rd. Urbana, IL USA,
E-mail: pega@illinois.edu

ABSTRACT

The paper presents the phenomenon of periodically reversing flow in a microchannel evaporators used in air conditioning systems which will be illustrated with high speed videos in the presentation. These evaporators have multiple parallel channels between 0.5 and 1mm and headers (manifolds) that have to accommodate tubes of typically 15 to 25 mm major (width).

A simultaneous flow visualizations and pressure measurements confirmed the periodic flow reversal and associated fluctuations. The oscillatory behavior of the flow is linked and related with oscillations of the evaporator pressure in the inlet header and the pressure drop. Visualization of the flow in headers and tubes will be presented.

Paper will present experiments that have revealed significant ratio of reversed vapor flow – in the range of 3-7% of the mail flow, in addition to liquid that is reversed alongside.

The magnitude and frequency of oscillations are directly proportional to heat flux.

Three potential impacts of flow reversal on evaporator performance are discussed: 1) moderate liquid maldistribution; 2) reduced heat transfer; 3) increased refrigerant side pressure drop.

Finally, to mitigate impacts of periodic reverse flow, a solution is proposed: to vent and bypass backflow vapor accumulated in the inlet header.

INTRODUCTION

Due to increased heat flux densities and reduced channel size, reverse vapor flow and boiling oscillation is a very noticeable problem in microscale heat exchangers with parallel flow. Extensive studies in past decades have identified several typical modes and underlying mechanisms, such as rapid bubble growth, parallel channel instabilities, and upstream compressible flow instability [1-5]. Nevertheless, to the authors' best knowledge there was no study or even indication of such phenomena in refrigeration and A/C microchannel evaporators with except of the information from CTS [6].

In microchannels, nucleation bubble can easily grow up to a size comparable to the channel hydraulic diameter. Further bubble growth becomes confined by the channel walls, only expanding in a longitudinal direction along the channel in a form of an elongated bubble. Such rapid bubble nucleation as well as confined expansion may introduce a pressure spike in the flow which may overcome the inertia of the incoming flow and the pressure in the inlet header, which in turn cause trailing edge of the bubble expanding upstream, i.e. a reverse flow [7]. However, this phenomenon seldom occurs in a large conventional tube, since the local high pressure generated by a single bubble is confined to a small region of the channel and can hardly affect the global pressure distribution and the bulk flow dynamics [4]. Kew and Cornwell [8] proposed a threshold of the bubble growth confinement based on the parameter, that is, Confinement number Co, and set the threshold at Co = 0.5. Meanwhile, inlet header serves as a buffer tank, providing significant compressible volume upstream of the heated microchannel tubes as well as an opportunity to effectively temporary stop the flow in some channels because others are available for increased flow rates. Such volume may be able to intermittently retain and discharge the backflow vapor, and thus dynamic boiling instability will be sustained by interactions between tube vapor generation and the upstream compressible volume [9]. Reverse vapor flow in parallel microchannels will cause the flow maldistribution, as vapor-liquid interface in each channel may temporally extend into different directions, either forward or backward [10-11]. Bogojevic et al. [12] deduced similar behavior in a group of 40 channels in which some had subcooled wall temperatures indicating single-phase flow, others were superheated indicating boiling.

Related work is summarized in Table 1 in Appendix. Wu and Cheng [2] found the temporal alterative appearance of two-phase flow and single-phase liquid flow, and regarded out-of-phase oscillations of pressures and mass fluxes as the cause for sustained instability. Brutin et al. [1,13] demonstrated that the presence of the buffer tank upstream the channel aggregates flow reversal and pressure drop oscillation with greater amplitude and lower frequency for n-pentane boiling in a single minichannel (Dh=889 μm). Hetsroni et al. [3,14] observed periodic wetting and rewetting boiling in triangular microchannel heat sink. The period between successive cycles of reversal flow includes four time intervals, and the dimensionless period decreases with increasing the boiling number. Chang and Pan [15] observed bubble slug oscillating growth leading to instances of reverse flow in 15 parallel microchannels (Dh=83.9 μm), and suggested that the magnitude of the pressure drop oscillations can be used as an index for the appearance of reverse flow.

Some researchers have presented approaches for reducing reverse vapor flow and stabilizing flow boiling in microchannels, as summarized in Table 2 in Appendix. So far, methods explored include: 1) raising inlet and system pressure by placing inlet area restriction of the microchannels [10, 24-27]; 2) using expanding channels with diverging cross-section design in which the steep pressure gradient near the inlet helps resist the reverse vapor flow[28-31]; 3) reducing the wall superheat and decelerating bubble growth rate by fabricating artificial nucleation sites on the channel walls [21,25,32-33]; 4) it was also found that flow boiling can be stabilized by actively generating initial seed bubbles to reduce wall superheat required for bubble nucleation, either by injecting additional gas or adding pulse voltage signal [34-26].

All studies listed in Table 1 and 2 were mainly focused on microchannel heat sinks for potential applications of small scale cooling systems. To the best knowledge of authors', no study or even indication of such phenomena like reverse flow in refrigeration and A/C microchannel evaporators were found in open literature, with exception of work at CTS [6]. Heat transfer and flow conditions for those microchannel heat sinks are significantly different from air-conditioning systems. The heat flux is usually controlled constant (up to about 1000 kW/m2) that is significantly higher than in evaporators of refrigeration and A/C systems. Flow starts with subcooled liquid at the inlet ending up with very low quality at exit in order to maintain two phase flow regime with high heat transfer coefficient in entire microchannels, while A/C and refrigeration systems are typically with superheat control and therefore refrigerant at the evaporator exit is very often in superheated vapor flow. Water is used in most experiments as the coolant and it has different thermophysical properties from typical refrigerants of R134a and R410A, such as vapor/liquid density, latent heat of vaporization, surface tension, and etc. Very recently, Bowers et al. [6] reported reverse flow in a microchannel evaporator used for a R410A residential A/C system operating in a direct expansion (DX) mode. Tuo and Hrnjak [37] identified three major impacts of the periodic reverse vapor flow on the microchannel evaporator: 1) moderate liquid maldistribution; 2) reduced overall heat transfer coefficient on the refrigerant side; 3) increased pressure drop across microchannel tubes.

Those methods found in open literature to suppress the reverse flow and boiling oscillation require sophisticated microscale manufacturing process which seems to be difficult or even feasible to apply in Al brazed microchannel heat exchangers used in mobile and stationary heat exchangers for capacities 1- 100 kW. In addition, there was no study to characterize and quantify the periodic reverse vapor flow from the heated microchannels. This would be very important information to further investigate the mechanism and impact of the flow boiling fluctuations induced by the periodic reverse vapor flow in microchannels.

The objective of this paper is to 1) propose a new method to reduce the reverse flow impacts on the performance of microchannel evaporators used in A/C systems; 2) demonstrate the benefits of venting the reverse vapor flow; 3) quantify the periodic reverse vapor flow.

NOMENCLATURE

$A_{\Delta P}$	[kPa]	ΔP fluctuation amplitude
A_s	[m^2]	heat transfer area
A_c	[m^2]	cross sectional area
D_h	[mm]	hydraulic diameter
f	-	frame number
F	[frame/s]	frame rate
G	[$kg \cdot m^{-2} \cdot s^{-1}$]	mass flux
	[$g \cdot s^{-1}$]	mass flow rate
p	[pixel]	image pixel
P	[kPa]	pressure
q	[$kW \cdot m^{-2}$]	heat flux
t	[s]	time
T	[ºC]	temperature
U	[$m \cdot s^{-1}$]	velocity
x	[-]	refrigerant quality

Special characters

τ_p	[s]	oscillation period
τ_1	[s]	liquid rewetting period
τ_2	[s]	transient annular film evaporating/dewetting period

Subscripts

avg	average value
a/air	indoor air side
e/evap	microchannel evaporator
FGBR	revised flash gas bypass
in	Inlet
out	Outlet
liq	liquid phase
ref	refrigerant side
rev	reverse flow
tot	total

FACILITY

Fig. 1 shows a schematic diagram of R134a A/C system in the test facility. It consists of a fixed displacement variable speed compressor, a microchannel condenser with an integrated receiver, a microchannel evaporator, and a manually-controlled electric expansion valve. The system is placed in two environmental chambers. Detailed information for major components can be found in previous study [38].

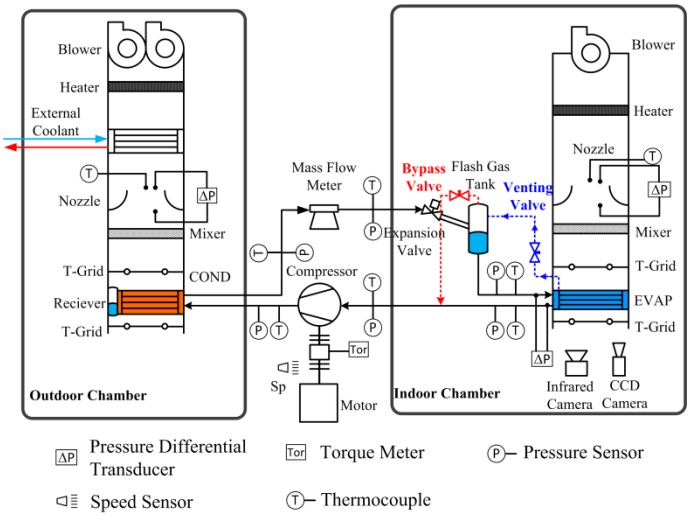

Figure 1. Schematic drawing of the test facility

Fig. 2 shows the detailed setup of microchannel evaporator section and revised flash gas bypass approach. To visualize the behavior of two-phase refrigerant flow within the inlet header, the original aluminum headers of the microchannel evaporator were cutoff and replaced by transparent ones made by transparent PVC tubes. The evaporator consists of totally 25 parallel flat tubes with a total face area of about 0.065 m2 and total air-side surface area of about 1.607 m2. Each flat tube has an effective heat transfer length of 260 mm and 10 parallel microchannels with the inner hydraulic diameter of 1.0 mm. Refrigerant flows upward along the vertical microchannel tube while air flow is perpendicular to the refrigerant flow direction, therefore forming a cross-flow configuration.

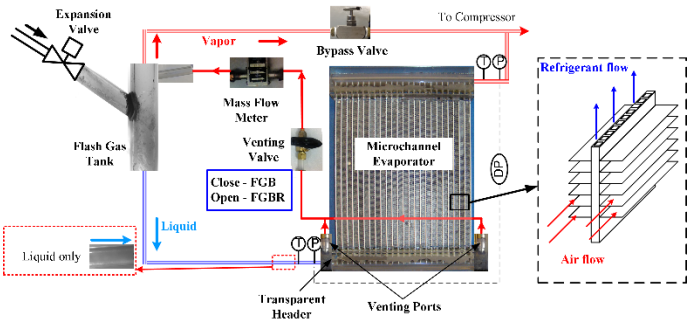

Figure 2. Detailed setup of evaporator section and revised flash gas bypass approach

Only liquid refrigerant is fed into the inlet header since flashing vapor generated during the isenthalpic expansion process is separated in the flash gas separator and bypassed to the compressor suction line. Thus, quality maldistribution due to flashing vapor is essentially eliminated by flash gas bypass (FGB) approach. FGB cycle is served as the baseline to quantify the impact of periodic reverse vapor flow on the evaporator and system performance. To get rid of the reverse vapor flow and therefore reduce its impact on the evaporator performance, two venting ports on both ends of the inlet header are added and let out the reverse vapor trapped in the inlet header back to the upstream flash gas separator. A mass flow meter with low pressure drop is installed on the venting line to measure the dynamic flow rate of the reverse vapor flow. This venting valve controls the flow resistance on the adiabatic venting line, preventing liquid entrainment from the inlet header and assuring accurate measurement of vapor flow. This method of venting out the reverse vapor flow is referred as Flash Gas Bypass Revised (FGBR) method. The detailed description of this FGBR method and its effects on the overall A/C system can be found in previous study [39].

An infrared camera measured the evaporator surface temperatures, which provides indirect information regarding refrigerant distribution inside parallel microchannel tubes. A high-speed CCD camera visualized the flow regime at the inlet header at a recording speed of 1000 fps. Meanwhile, a high-speed datalogger used at a sampling rate of 100 Hz recorded simultaneous oscillations of the inlet/outlet pressures measured by two pressure sensors and the pressure drop measured independently by a pressure differential transducer. Table 3 lists the test conditions of the microchannel evaporator in this A/C system. The uncertainties for pressure, temperature and mass flow rate measurements are about ± 3.56 kPa, ±0.5 ºC and ±0.1%, respectively.

Table 3. Operating conditions

Items	Unit	Condenser side	Evaporator side
Air inlet temperature	ºC	27 35 43	27 35 43
Air volume flow	m^3/s	0.342	0.233
Face air velocity	m/s	1.25	3.64
Relative humidity	-	-	Dry
Compressor speed	rpm	900	

RESULTS

In this section, effects of the periodic reverse vapor flow will be studied by comparing evaporator performances without (FGB) and with (FGBR) venting the reverse vapor flow in terms of flow regime in the inlet header, evaporator surface temperature profile, dynamic behaviors of the pressure drop and inlet pressure.

Effects on the flow regime in the inlet header

Fig. 3 compares the flow regimes at three different locations along the inlet header without and with venting the periodic reverse vapor flow trapped in the header. Although FGB cycle feeds the evaporator with liquid only refrigerant, as flashing vapor generated during the expansion process is separated and bypassed to the suction line (Fig. 2), the inlet header is not yet filled up with liquid. A clear vapor-liquid interface distinguishes the liquid pool at the bottom and a vapor pocket at the top, oscillating up and down around the tube inlets and making waves in horizontal direction. This is the direct consequence of the reverse vapor flow which is periodically discharged out of the heated channels and stored at the inlet header. While, it is evident that venting the reverse vapor flow almost removes the vapor pocket occupying the top portion of the header and elevates the vapor-liquid interface. All the mouths (ports) of microchannel tubes are submerged in the liquid pool. Despite of still existence of periodic reverse vapor flow, the buoyancy force will cause backflow bubbles to quickly rise and vent out of the inlet header. Each channel will always take in liquid refrigerant when the upward liquid flow is re-instated. It essentially eliminates the temporal liquid maldistribution which is occurred in the FGB cycle (without venting) due to oscillating vapor-liquid interface. In addition, almost no reverse vapor is observed to be re-entrained back into the tubes based on flow visualization, and thus local refrigerant-side heat transfer coefficient will be increased by removing those entrained bubble slugs in FGB cycle.

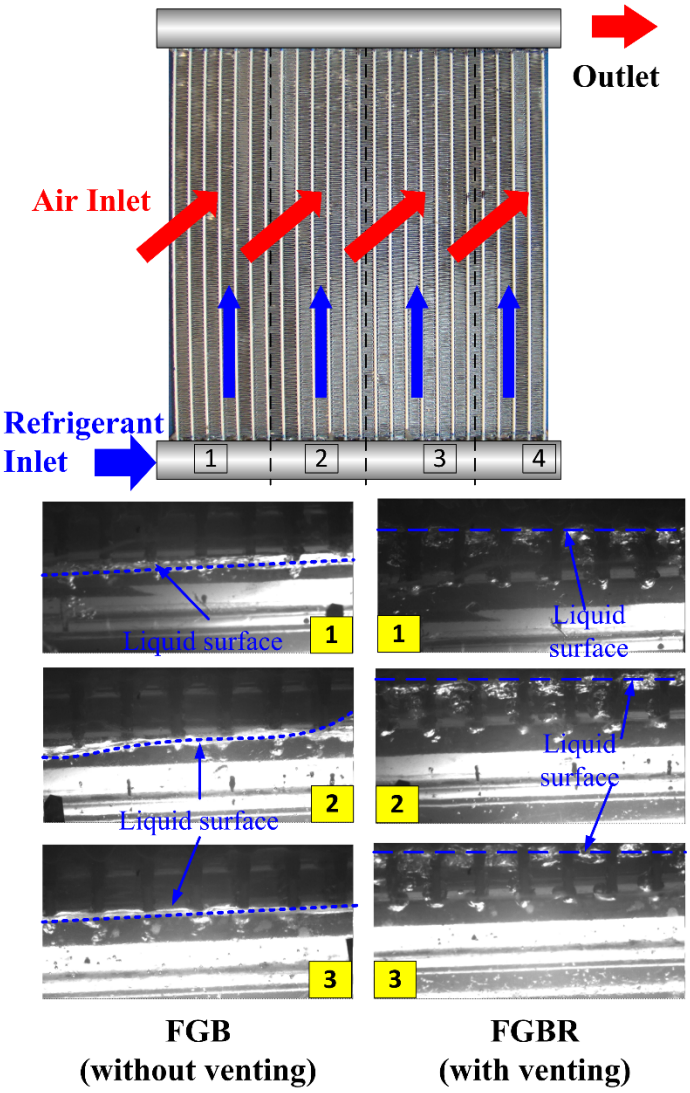

Figure 3. Effect of venting the reverse vapor flow on the flow regime at the inlet header

Fig. 4 shows a sequence of frames from a high-speed video depicting the periodic reverse flow observed at one portion of the inlet header. In the FGB cycle, the bubbles are gradually discharged out of the tubes against upward bulk flow direction, rising up in the liquid pool driven by the buoyancy force, and finally breaking up and merging into the vapor pocket occupying the top portion of the inlet heater. As the backflow vapor generated within the heated microchannels is continuously accumulating in the header, the volume of the vapor pocket is expanding, and expelling out liquid refrigerant retained at the header bottom. Therefore, it can be seen that the level of vapor-liquid interface gradually drops. Until about t+1.2 s, the interface drops down to the lowest level and reverse vapor flow seems reduced. Afterwards, forward upward flow is re-instated since the inlet pressure is sufficient to overcome the pressure drop along the microchannel tubes. However, because the vapor pocket is present above the liquid pool which interface is below the tube inlets, most likely only vapor refrigerant is received by tubes at the beginning. When rising liquid surface reaches the tube inlets, fresh liquid starts to feed the microchannels. From above observation and analysis, the period of one oscillation cycle is estimated about 1.8 s. However, in the FGBR cycle with vapor venting, the liquid surface is elevated, which in turn results in the vapor pocket with a reduced size. The vapor-liquid interface seems relatively stable with no discernible up-down oscillation, because the reverse vapor is discharged out without considerable accumulation in the header.

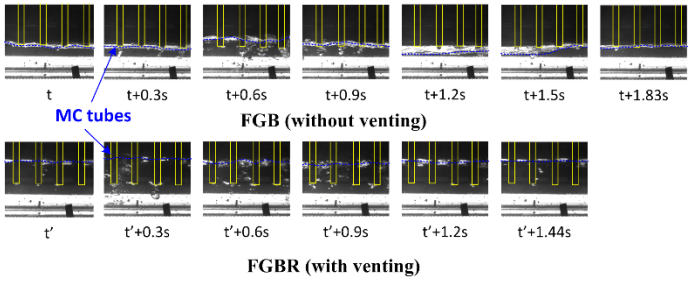

Figure 4. Sequential high speed images of flow regime at the inlet header

Effects on the evaporator surface temperature

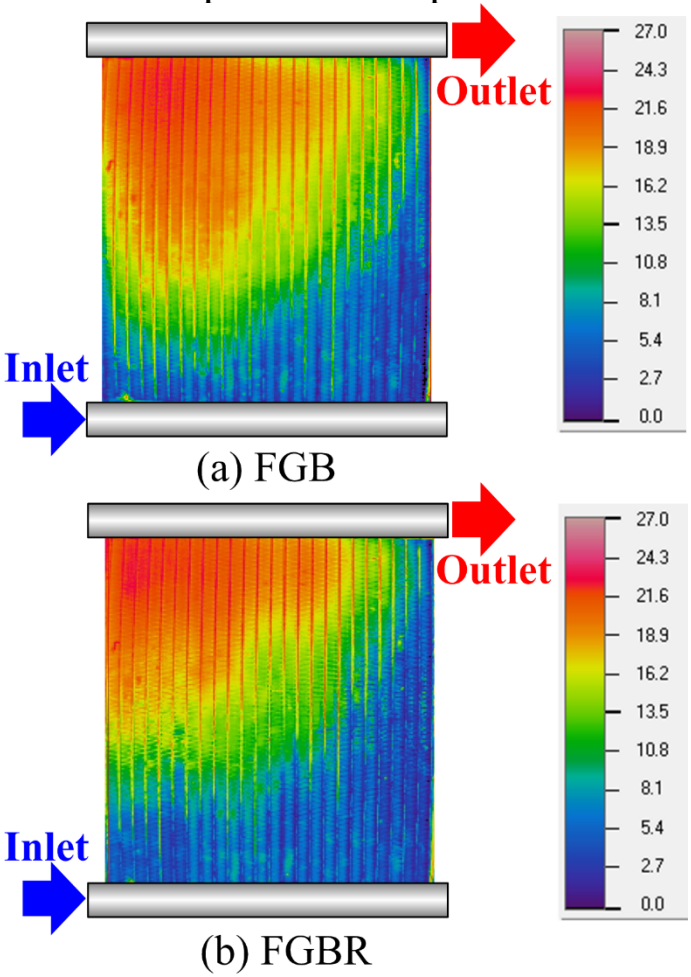

Figure 5. Evaporator surface temperature profiles in three cycles at 27/27 °C condition
(a) FGB (ϕ=0.795); (b) FGBR (ϕ=0.828)

The surface temperature profile usually provides indirect indication of the refrigerant distribution inside parallel microchannel tubes, since tubes receiving lesser liquid refrigerant flow will end up with earlier dryout or a larger superheated region. Typically, more uniform and smaller superheated region indicates more uniform refrigerant distribution among parallel tubes. Fig. 5 depicts the evaporator surface temperature profiles in FGB and FGBR cycles at 27/27 °C condition. It is evaluated and compared quantitatively by the distribution rating parameter ϕ proposed by Bowers et al. [40]. ϕ is based on evaporator surface temperature and its shape. An isotherm is defined by averaging the temperature values at each pixel point as following:

$$T_{iso} = \frac{\sum T_i}{N \times M} \tag{1}$$

Where N and M are number of image pixels at each row and column.

Once Tiso is determined for a given infrared image, the image is divided into columns of pixels. For each column i, the number of pixels with temperature below Tiso is determined to define a height (Hi) and therefore the average height of all the columns (Havg). Thus, distribution rating parameter ϕ represents the arithmetic deviation of individual height away from the average one, and defined as following:

$$\phi = 1 - \frac{\sum_{i=1}^{N} \left| H_i - H_{avg} \right|}{2nH_{avg}} \tag{2}$$

ϕ closer to 1 indicates more uniform distribution. The rating parameter ϕ is 0.828 in FGBR cycle, 4.2% higher than 0.795 in FGB cycle. This confirms an improved refrigerant distribution by removing the reverse vapor trapped in the inlet header and therefore feeding only liquid refrigerant to each microchannel tubes. It should be noted that in FGBR cycle the microchannel tubes at the rear end of the header appear to receive more liquid refrigerant than those close to the inlet as seen a smaller superheated zone (red color). The main reason is the mass flow maldistribution caused by the pressure drop of the outlet header [41], [42].

To compare the temporal oscillations, surface temperatures at three locations (1/4th, 1/2th, and 3/4th) along 8 and 12 microchannel tubes in both FGB and FGBR cycles at 35/35 °C conditions are shown in Fig. 6(a) and (b). The oscillation amplitudes of surface temperatures in FGBR cycle is less than 1 °C, much smaller than the corresponding FGB cycle with up to 3 °C oscillation. This indicates more stable two-phase flow and heat transfer within the microchannel tubes when venting the reverse vapor trapped in the inlet header, which in turn contributes to the improved heat transfer performance of the microchannel evaporator. Besides, the oscillation in FGBR cycle is in a faster speed, the period is estimated only about 1.4 s, much lower than about 2.0 s period in FGB cycle.

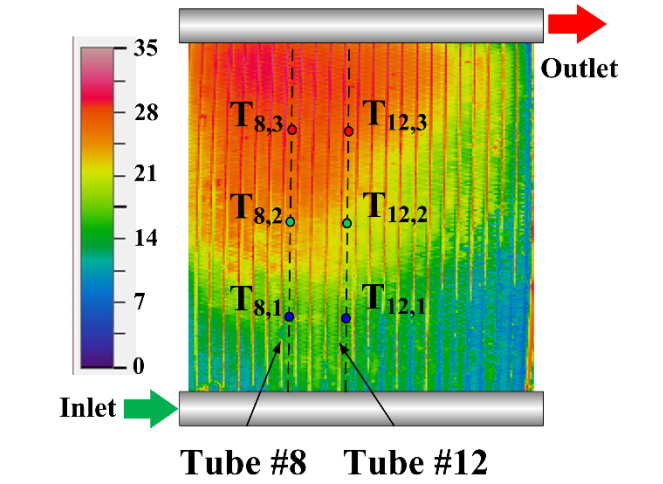

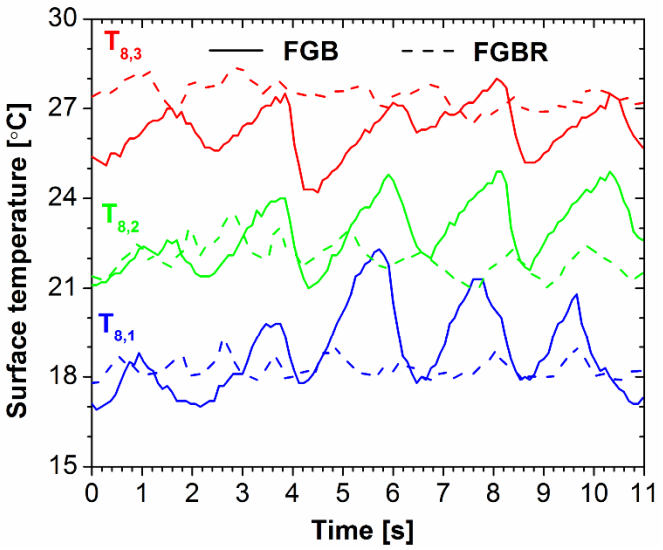

(a) Tube #8

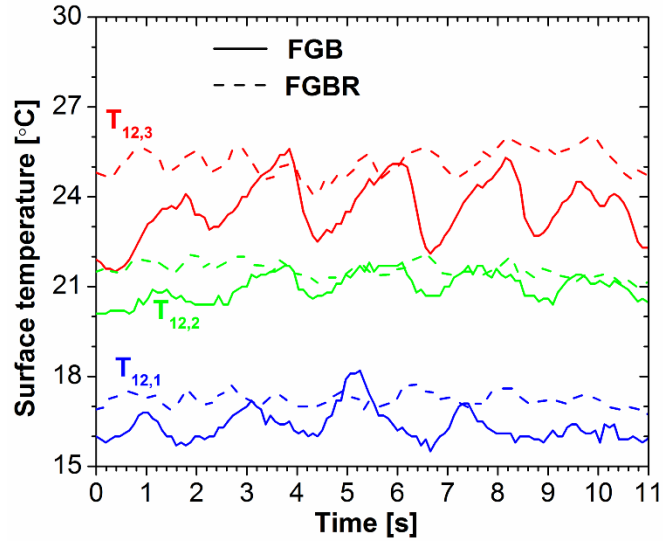

(b) Tube #12

Figure 6. Temporal oscillations of evaporator surface temperatures of microchannel tubes

Effects on the pressure and pressure drop oscillations

Behavior of the periodic reverse vapor flow could be indicated by oscillations of pressure, flow rate and temperatures in microchannels [1, 3, 16, 19]. Fig. 7 illustrates temporal oscillations of evaporator inlet/outlet pressures and overall pressure drop in both FGB cycle (without vapor venting). In order to characterize the oscillation, Fast Fourier Transform (FFT) analysis is used to convert time-dependent data (Fig.7 (1a) and (2a)) into corresponding frequency domain data (Fig.7 (1b) and (2b)), in which dominant frequency, if any, and amplitude could be identified.

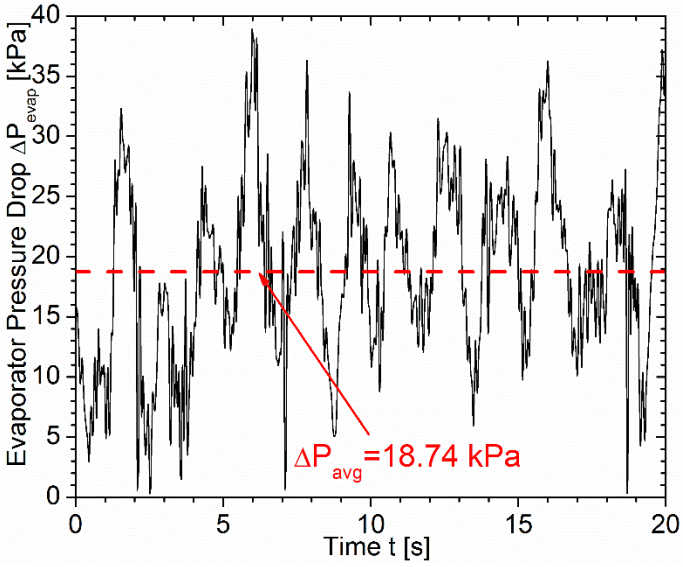

(1a) pressure drop fluctuation;

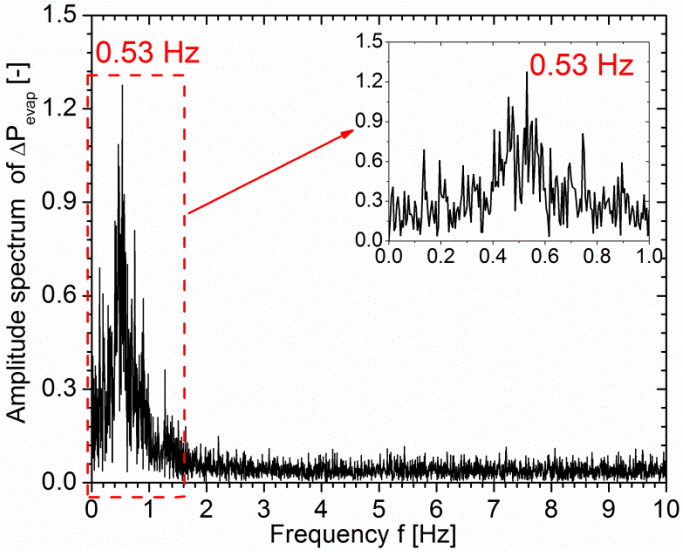

(1b) pressure drop amplitude spectrum;

In FGB cycle, the evaporator pressure drop is about 18.65 kPa in average but temporally varies between the instant maximum of about 39 kPa and the minimum of almost 0 kPa, resulting in the peak-to-peak amplitude of roughly 39 kPa. In frequency domain, ΔP spectrum only has one dominant frequency band centered at 0.53 Hz. This peak value corresponds to a period of 1.89 s, which approximately corresponds to that of periodic reverse flow observed in Fig. 4 and of surface temperature oscillations in Fig. 6. It is interesting that Pin FFT shows exactly the same dominant frequency band and the peak frequency, but Pout remains almost constant. These results confirm that oscillations of pressure and surface temperature are caused by the interaction of the reverse vapor flow generated within the microchannels and the compressible volume of the inlet header.

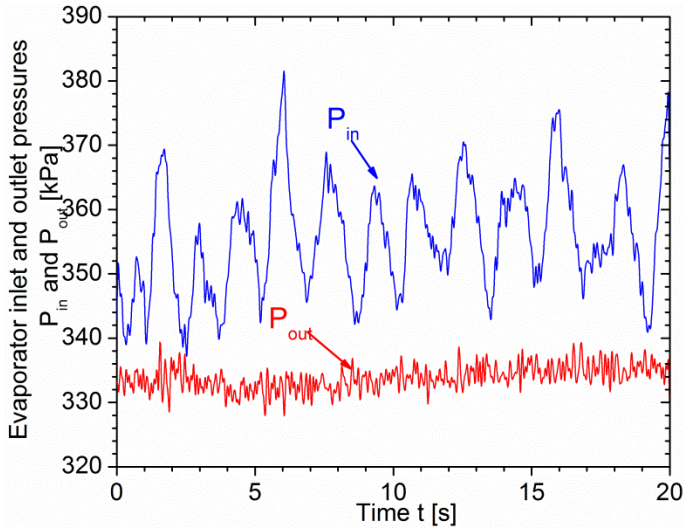

(2a) inlet and outlet pressure oscillations;

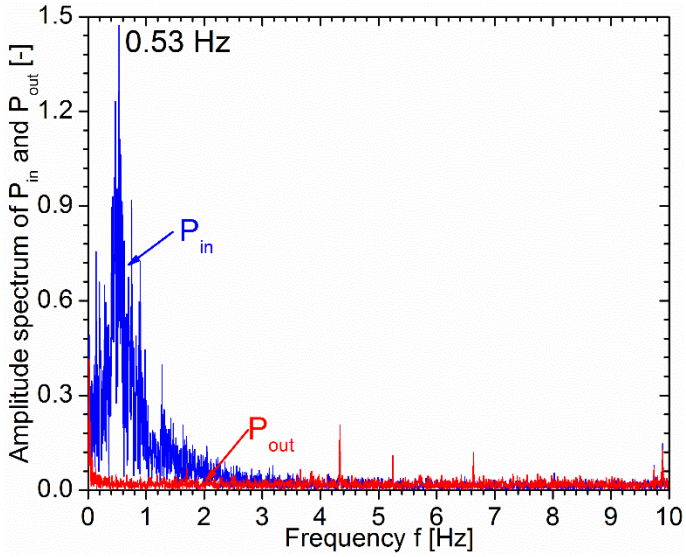

(2b) inlet and outlet pressure amplitude spectrum

Figure 7. Variation of evaporator inlet/outlet pressures and pressure drops in FGB cycle at 35ºC/35 ºC condition

The average wall heat flux and refrigerant mass flux in the microchannel evaporator are defined as:

$$q_{avg} = \frac{Q_e}{A_{ref,s}} \qquad (3)$$

$$G_{avg} = \frac{\dot{m}_{ref}(1-x_{in})}{A_{ref,c}} \quad (4)$$

where Qe, $\dot{m}_{ref}$, xin are the cooling capacity, the total refrigerant mass flow rate and quality right after the expansion valve. Aref,s and Aref,c denote the total heat transfer surface area and microchannel cross sectional area on the refrigerant-side. It should be noted that $\dot{m}_{ref}(1-x_{in})$ is the mass flow rate of liquid only refrigerant since flashing vapor is separated and bypassed in the upstream separator (see Fig. 2).

Three sets of ambient temperatures on the condenser and evaporator side result in different cooling capacities and corresponding liquid refrigerant mass flow rates through the evaporator. In general, when the A/C system compressor speed is fixed, average heat flux and refrigerant mass flux increase with air inlet temperature due to the increased air-refrigerant temperature difference. It should be noted that the local heat flux and mass flux in each channel are different due to the existing flow maldistribution induced by header pressure drop and resultant superheated area. Thus, qavg and Gavg only give a rough estimation of boiling conditions in the microchannel evaporator.

Fig. 8 compares the time-wise average of the evaporator pressure drop with and without vapor venting at three air inlet temperatures as a function of the average refrigerant mass flux. It is evident that venting the reverse vapor flow out of the inlet header reduces the pressure drop about 10% – 15% in the FGBR cycle, as the reverse vapor is bypassed around the evaporator through the adiabatic venting line, instead of recirculating back and forth between the heated channels and the inlet header.

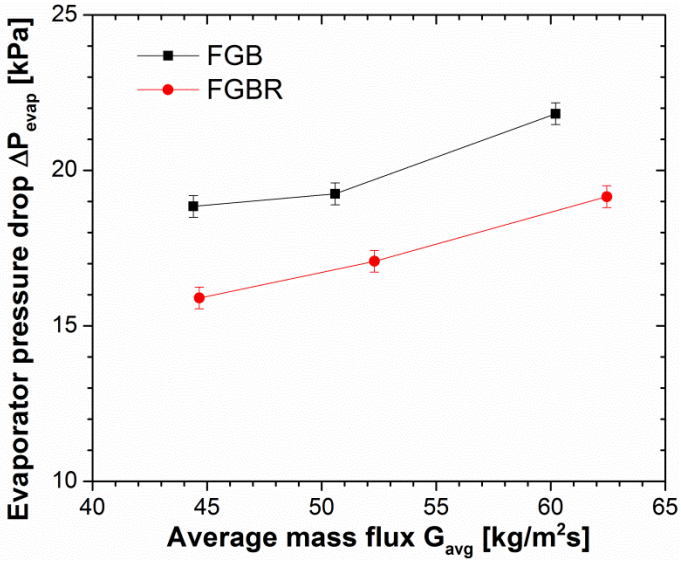

Figure 8. Pressure drop reduction by venting the reverse vapor as function of average mass flux

Fig. 9(a) and (b) show effect of venting the reverse vapor on the oscillation amplitude and period of the evaporator inlet pressure. It can be seen that vapor venting reduces the inlet pressure oscillation amplitude up to 8 kPa, which is corresponding to about 0.7 °C fluctuation of inlet saturation temperature. This is mainly because removing vapor reduces the quantity of the backflow vapor temporarily stored in the vapor pocket within the header (See Fig. 4) and affects the resultant pressure change. An increase in heat flux applied on the microchannels results in a decrease of the pressure oscillation period in both cases, but it appears faster and less sensitive with the heat flux in the case of vapor venting. Reduced oscillation period may be due to two facts. First, vapor venting would facilitate the backward progression of bubble elongation from the heated microchannel tubes back to the header. As illustrated in Fig. 4, when venting the reverse vapor liquid surface appears to be more stable and smooth.

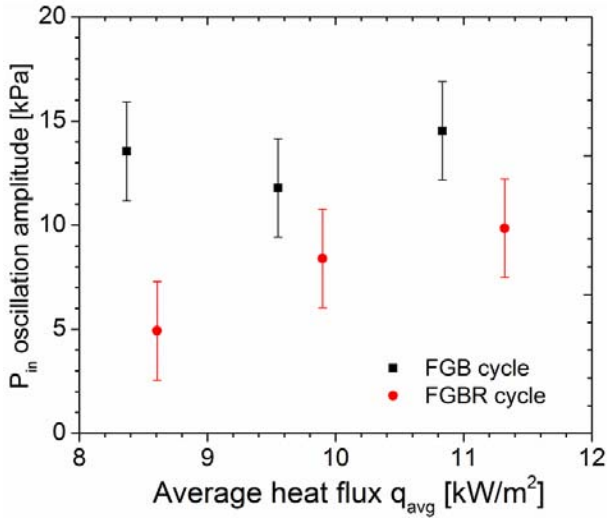

(a) Oscillation amplitude

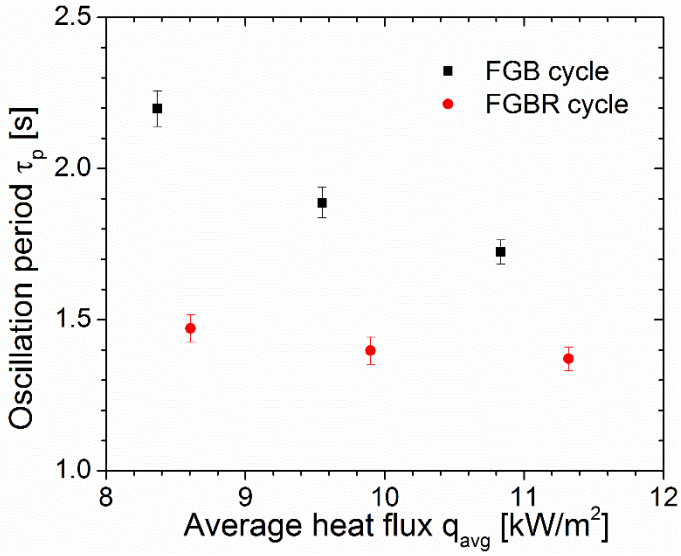

(b) Oscillation period

Figure 9. Comparison of inlet pressure oscillations in FGB and FGBR cycles as a function of average heat flux

Characteristics of the periodic reverse vapor flow

In the FGBR experimental system, the mass flow meter situated on the venting line measures the mass flow rate of the reverse vapor refrigerant removed from the inlet header (see Fig. 2). Careful inspection on certain high speed images (Fig. 4 in t+1.2 s and t+1.5 s) indicates that not only vapor is returned, but also some liquid in the form of droplets or ligament drips out of the microchannels. Unfortunately, the mass flow meter is not able and not intended to measure that portion of returned liquid flow because it never shows in the venting line. Fig. 10 illustrates temporal oscillations and corresponding amplitude spectrums of inlet and outlet pressures, and mass flow rate of vented reverse vapor. The vented vapor flow rate is synchronized with the inlet pressure. Both their amplitude spectrums peak at the same dominant frequency of about 0.7 Hz, which is corresponding to a period of about 1.43 s.

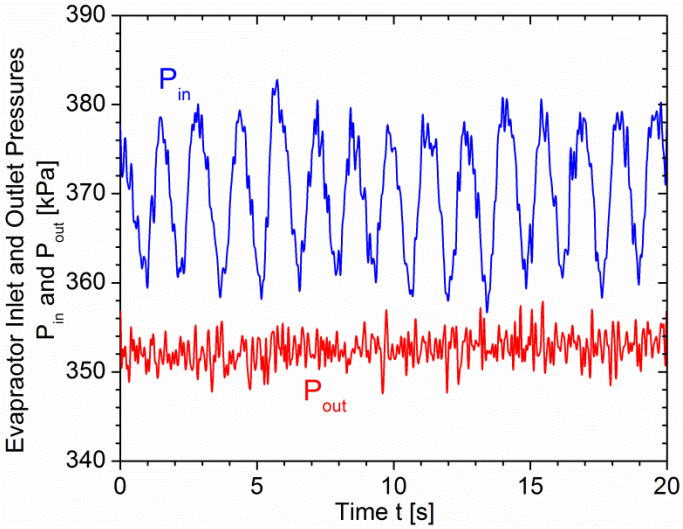

(1a) Oscillations of inlet and outlet pressures

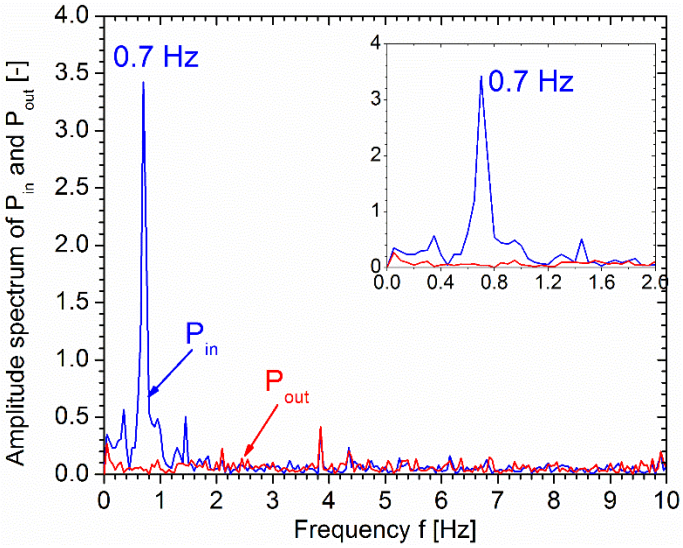

(1b) Amplitude spectrum of inlet and outlet pressures

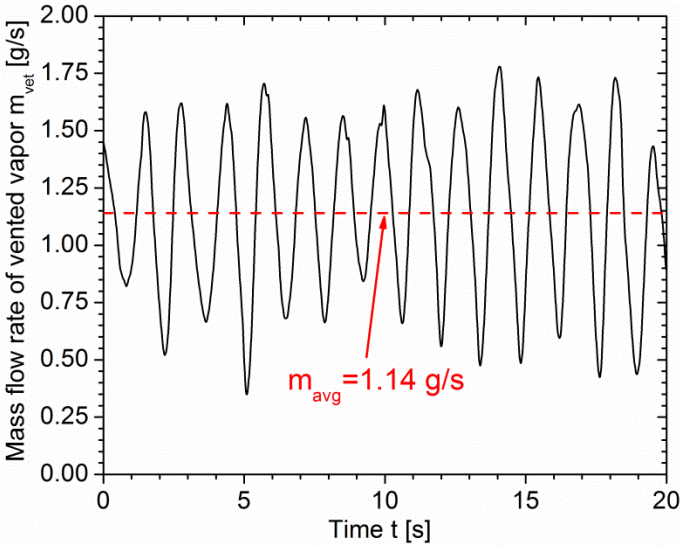

(2a) Oscillations of vented vapor mass flow rate

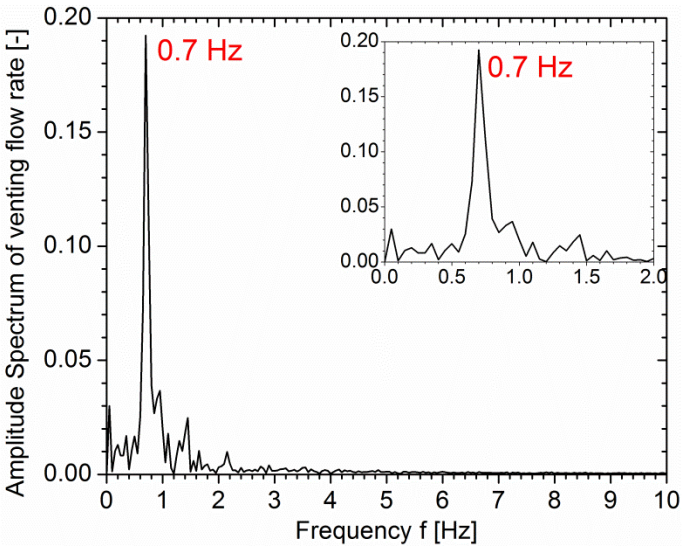

(2b) Amplitude spectrum of vented vapor flow rate

Figure 10. Temporal oscillations of measured pressures and vented vapor flow rate at 35°C/35°C condition

However, vented vapor flow rate is always greater than zero, indicating the continuous vapor venting. But, it is expected that the reverse vapor flow at each microchannel is intermittent and will be ceased when upward liquid flow refills the channels. Mass conservation law supports the equivalence of time-wise average of the vented vapor flow rate with that of the total reverse vapor generated within all the channels, while they are not dynamically equivalent to each other. That is the consequence of the fact that vented flow is the function of the pressure difference between inlet header and point of connection at the exit. Vapor reversed from the tube affects the pressure in the inlet header and thus the vented flow. In addition, it can be explained by inspecting the dynamic behavior of the reverse vapor flow.

The vapor reversal from each microchannel does not exactly follow the same dynamics. Among the total 250 parallel microchannels, flow may occur in opposite directions either in adjacent channels within the same flat tube or in two channels situated at two different tubes as the bubble nucleation followed by axial growth is weakly correlated among channels. For instance as shown in Fig. 4, at t′+0.3 s, three tubes on the left inject the bubbles with different sizes into the liquid pool, while the one on the right has no sign of backflow.

Similarly, Fig. 11 shows sequential images of backflow bubbles recorded at ten ports of #8 microchannel tube. The emphasis is on the effect of location of the channels in air stream direction. Air flow comes from the right to the left and its temperature gradually decreases as being cooled down by the refrigerant flow within the microchannels. Due to the air temperature glide, the leading channel on the right receives higher heat flux than the trailing channel although the transverse heat conduction through aluminum wall reduces the difference of heat flux among parallel channels. Clearly, flow reversals are not related, as it can be seen that some channels discharge out bubbles (marked by dash box) while others do not at a particular instant, indicating that flow may occur in opposite directions in adjacent channels. In addition, it seems that in one cycle the reverse bubbles appear slightly earlier in the trailing channel than in the leading channel. The sequence of the flow reversal in each channel does not correspond to the magnitude of applied heat flux. That also indicates strong effect of conduction through the metal of the tube in direction of air flow. Such somewhat random behavior of the vapor reversal is also observed visually and reported by other scholars [11, 26, 43].

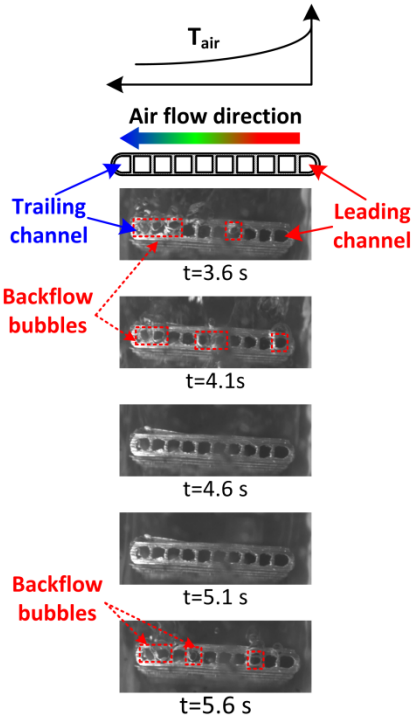

Figure 11. Sequential images of backflow bubbles at ten parallel ports of #8 microchannel tube (27/27 °C air temperatures). Arrow indicates the air flow direction from right to left

On the other hand, a vapor pocket in the header is still present, but with a reduced size compared to the FGB cycle. It creates a passage to transfer the reverse vapor towards the two venting ports. Its presence will inevitably buffer the oscillation amplitude of the reverse vapor flow rate. Both effects contribute to the non-zero or continuous venting of the reverse vapor flow.

The reverse vapor flow is characterized by average flow rate, oscillation amplitude and period. The average vented vapor flow rate is the time-wise mean value, defined as following:

$$\dot{m}_{vet,avg} = \frac{\int_0^T \dot{m}_{vet} dt}{T} \tag{5}$$

where $\dot{m}_{vet}$ and T are instant vented vapor flow rate and the total recording time interval.

Oscillation amplitude is defined as the average of half the peak-to-trough difference with each oscillation:

$$\Delta\dot{m}_{vet,avg} = \frac{\sum_{i=0}^{N}\left(\left(\dot{m}_{vet,\max}\right)_i - \left(\dot{m}_{vet,\min}\right)_i\right)}{2N} \tag{6}$$

where N is total number of the oscillation period during the recording interval T; $\left(\dot{m}_{vet,\max}\right)_i$ and $\left(\dot{m}_{vet,\min}\right)_i$ are the peak and trough values with the i-th oscillation, respectively.

It is complex to map the oscillation of vented vapor flow with average wall heat flux, because: 1) heat flux is hardly uniform even along the individual microchannel since refrigerant heat transfer coefficient varies significantly as quality increases; 2) the average inlet mass flux (defined by Eqn. (4)) also proportionally increases with the average heat flux (defined by Eqn. (3)), theoretically at an almost constant rate. Assuming that refrigerant exits the evaporator in saturated vapor, the cooling capacity of the evaporator can be expressed as:

$$Q_e = q_{avg} A_{ref,s} \tag{7}$$

$$Q_e = G_{avg} A_{ref,c} \Delta h_{fg} \tag{8}$$

For the current evaporator with rectangular shape microchannels, total refrigerant-side heat transfer area Aref,s and cross-sectional area Aref,c can be written as:

$$A_{ref,s} = 4 D_h L_t N_p N_t \tag{9}$$

$$A_{ref,c} = D_h^2 N_p N_t \tag{10}$$

Where Dh and Lt are microchannel hydraulic diameter and total tube length; Np and Nt are the number of channels in each flat tube and the number of parallel flat tubes.

Substituting Eqs. (8-10) into Eqn. (7) yields:

$$\frac{G_{avg}}{q_{avg}} = \frac{4L_t}{D_h}\frac{1}{\Delta h_{fg}} \qquad (11)$$

$\frac{G_{avg}}{q_{avg}}$

Eqn. (11) indicates that is approximately a constant value for a given size evaporator. Two variables cannot be varied independently. As shown in Fig. 12, this ratio is about 5.39, and all experimental results roughly fit on the theoretical value. Those error bars are based on the uncertainties of experimental measurements.

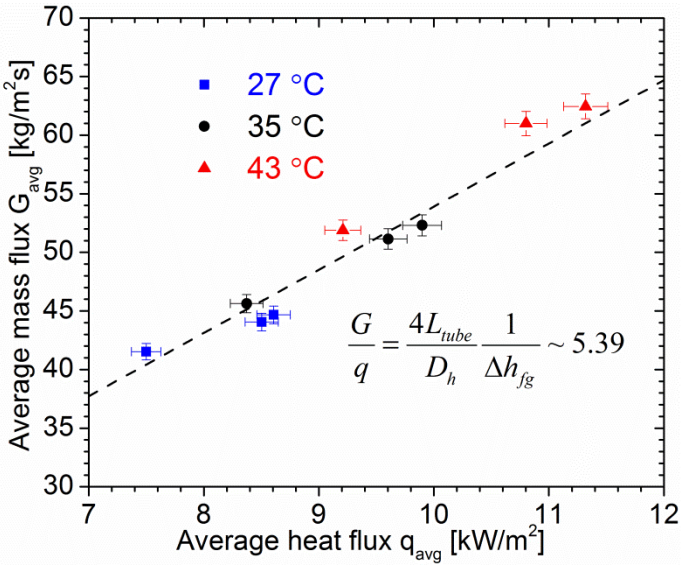

Figure 12. Relationship between average heat flux and mass flux at the microchannel tubes

Fig. 13 shows effect of the average wall heat flux on average vented vapor flow rate and its oscillation amplitude under three ambient conditions. Overall, it seems that both average vented vapor flow rate $\dot{m}_{vet,avg}$ and the oscillation amplitude $\Delta\dot{m}_{vet,avg}$ increase with the average heat flux qavg, but some data do not strictly follow the trend. This is because both heat flux and mass flux affects the dynamic behavior of the reverse vapor flow. In general, higher heat flux intensifies bubble nucleation followed by the longitudinal expansion and therefore increases the reverse vapor flow rate. On the other hand, greater mass flux intends to stabilize flow boiling by increasing incoming flow inertia and pressure drop resistance upstream the reverse vapor.

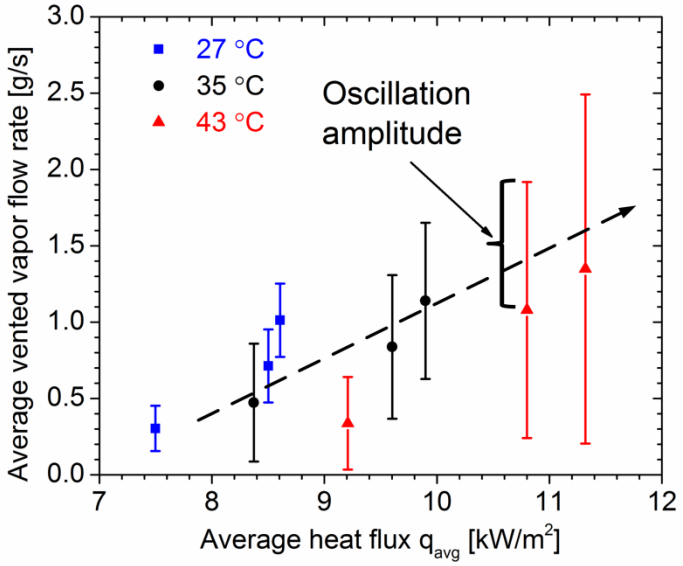

Figure 13. Variations of average vented vapor flow rate and its oscillation amplitude with average wall heat flux

Fig. 14 shows the ratio of vented reverse flow rate to the total refrigerant flow supplied to the evaporator, as an indicative of relative magnitude of the reverse vapor flow. The instant peak value is up to about 13% of the total inlet flow rate while the instant minimum is almost 0. The average vented vapor flow rate varies between about 8% to 2% at conditions explored in this study. Fig. 15 depicts characteristic oscillation period of the vented reverse vapor flow as a function of average heat flux. It decreases from about 2 s to 1.4 s with heat flux increasing, indicating a more intensive reverse vapor flow.

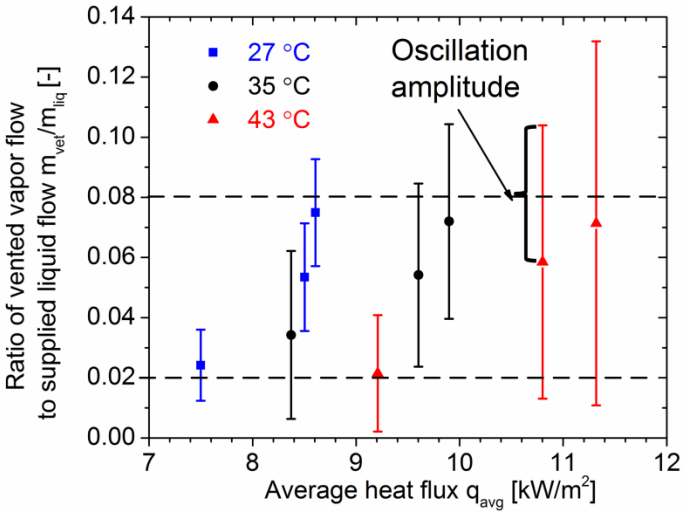

Figure 14. Ratio of the vented vapor flow rate to total inlet flow rate

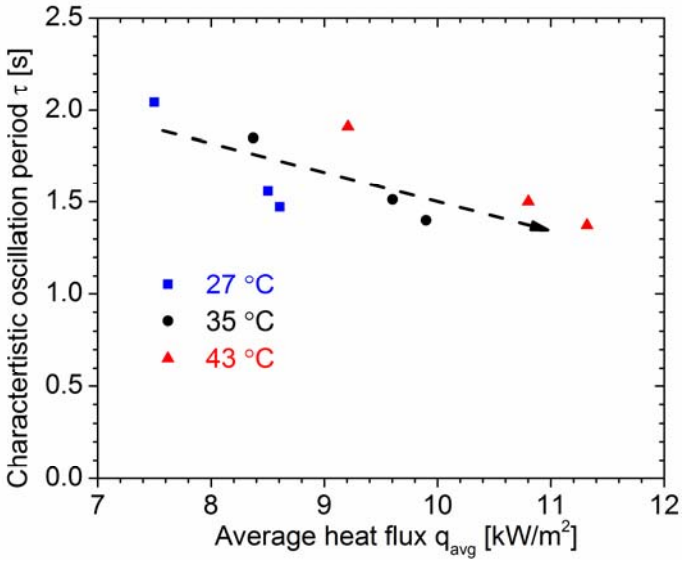

Figure 15. Oscillation period of the vented reverse vapor flow rate

CONCLUSION

This paper first described reverse flow in microchannel evaporators and then proposed a revised flash gas bypass (FGBR) as a way to mitigate its consequences. The idea is to vent the reverse vapor from the inlet header. Meanwhile, temporal oscillation of the reverse vapor flow is characterized through pressure oscillations in the header and evaporator. In addition the vented vapor flow rate was measured and related to the reverse flow.

By venting the reverse vapor out of the inlet header, the liquid level within the inlet header is stabilized compared to FGB (without venting) and elevated above all the tube inlets (see Fig. 3). Thus, compared to FGB system, liquid distribution becomes more uniform since each tube receives liquid only refrigerant when the forward flow is periodically re-instated (see Fig. 5).

Removing the reverse vapor reduces the oscillation amplitude and period of the inlet pressure. The evaporator pressure drop is further decreased because venting the reverse vapor decreases the refrigerant mass flow rate and average void fraction within the evaporator (see Fig. 8).

Vented reverse vapor mass flow rate oscillates periodically and in-sync with fluctuations of evaporator inlet pressure. Its temporal mean value and oscillation amplitude increase proportionally to average wall heat flux. The ratio of vented vapor flow rate to total inlet refrigerant flow rate varies in the range 8% to 2% at explored conditions of qavg = 7.5 ~ 11.5 kW/m2 and Gavg = 40 ~ 65 kg/m2s. Oscillation period increases from about 1.4 s to 2 s as average heat flux decreases.

Acknowledgement

We are grateful for financial and technical support from the Air Conditioning and Refrigeration Center (ACRC) at the University of Illinois and CTS.

REFERENCES

[1] D. Brutin, F. Topin, L. Tadrist, Experimental study of unsteady convective boiling in heated minichannels, Int J Heat Mass Transfer 46(16) (2003) 2957-2965.

[2] H.Y. Wu, P. Cheng, Visualization and measurements of periodic boiling in silicon microchannels, Int J Heat Mass Transfer 46(14) (2003) 2603-2614.

[3] G. Hetsroni, A. Mosyak, E. Pogrebnyak, Z. Segal, Explosive boiling of water in parallel micro-channels, Int J Multiphas Flow 31(4) (2005) 371-392.

[4] C.J. Kuo, Y. Peles, Flow boiling instabilities in microchannels and means for mitigation by reentrant cavities, J Heat Transfer 130(7) (2008) 072402-10.

[5] T.J. Zhang, T. Tong, J. Chang, Y. Peles, R. Prasher, M.K. Jensen, T. Wen, P. Phelan, Ledinegg instability in microchannels, Int J Heat Mass Transfer 52(25-26) (2009) 5661-5674.

[6] C.D. Bowers, H. Mai, S. Elbel, P.S. Hrnjak, Refrigerant distribution effects on the performance of microchannel evaporators, Int Refrig and Air Conditioning Conf at Purdue (2012) No.2173.

[7] S.G. Kandlikar, Nucleation characteristics and stability considerations during flow boiling in microchannels, Exp Therm Fluid Sci 30(5) (2006) 441-447.

[8] P.A. Kew, K. Cornwell, Correlations for prediction of flow boiling heat transfer in small-diameter channels, Appl Therm Eng, 17(8-10) (1997) 705-715.

[9] A.E. Bergles, S.G. Kandlikar, On the nature of critical heat flux in microchannels, J Heat Transfer 127(1) (2005) 101-107.

[10] W. Qu, I. Mudawar, Transport phenomena in two-phase micro-channel heat sinks, J of Electron Packaging, 126(2) (2004) 213-224.

[11] P. Balasubramanian, S.G. Kandlikar, Experimental study of flow patterns, pressure drop, and flow instabilities in parallel rectangular minichannels, Heat Transfer Eng 26(3) (2005) 20-27.

[12] D. Bogojevic, K. Sefiane, A.J. Walton, H. Lin, G. Cummins, D.B.R. Kenning, T.G. Karayiannis, Experimental investigation of non-uniform heating effect on flow boiling instabilities in a microchannel-based heat sink, Int J Therm Sci 50(3) (2011) 309-24.

[13] D. Brutin, L. Tadrist, Pressure drop and heat transfer analysis of flow boiling in a minichannel: influence of the inlet condition on two-phase flow stability, Int J Heat Mass Transfer 47(10-11) (2004) 2365-2377.

[14] G. Hetsroni, A. Mosyak, E. Pogrebnyak, Z. Segal, Periodic boiling in parallel microchannels at low vapor quality, Int J Multiphas Flow 32(10-11) (2006) 1141-1159.

[15] K.H. Chang, C. Pan, Two-phase flow instability for boiling in a microchannel heat sink, Int J Heat Mass Transfer 50(11-12) (2007) 2078-2088.

[16] H.Y., Wu, P. Cheng, Boiling instability in parallel silicon microchannels at different heat flux, Int J Heat Mass Transfer 47(17-18) (2004) 3631-3641.

[17] S.G. Kandlikar, P. Balasubramanian, Effect of gravitational orientation on flow boiling of water in 1054 x 197 μm parallel minichannels, ASME Conference Proceedings 41642 (2004) 539-550.

[18] J. Lee, I. Mudawar, Two-phase flow in high-heat-flux micro-channel heat sink for refrigeration cooling applications: Part I—pressure drop characteristics, Int J Heat Mass Transfer 48(5) (2005) 928-940.

[19] J. Xu , J. Zhou, Y. Gan, Static and dynamic flow instability of a parallel microchannel heat sink at high heat fluxes, Energ Convers Manage 46(2) (2005) 313-334.
[20] C. Huh, K. Jeongbae, M.H. Kim, Flow pattern transition instability during flow boiling in a single microchannel, Int J Heat Mass Transfer 50(5-6) (2007) 1049-1060.
[21] C.J. Kuo, Y. Peles, Pressure effects on flow boiling instabilities in parallel microchannels, Int J Heat Mass Transfer 52(1-2) (2009) 271-280.
[22] J. Barber, D. Brutin, K. Sefiane, J.L. Gardarein, L. Tadrist, Unsteady-state fluctuations analysis during bubble growth in a rectangular microchannel, Int J Heat Mass Transfer 54(23-24) (2011) 4784-4795.
[23] D. Bogojevic, K. Sefiane, A.J. Walton, H. Lin, G. Duursma, Two-phase flow instabilities in a silicon microchannels heat sink, Int J Heat Fluid Flow 30(5) (2009) 663-675.
[24] A. Kosar, C. Kuo, Y. Peles, Suppression of boiling flow oscillations in parallel microchannels by inlet restrictors, J Heat Transfer 128(3) (2006) 251-260.
[25] S.G. Kandlikar, W.K. Kuan, D.A. Willistein, J. Borrelli, Stabilization of flow boiling in microchannels using pressure drop elements and fabricated nucleation sites, J Heat Transfer 128(4) (2006) 389-396.
[26] P. Jung Eung, J.R. Thome, B. Michel, Effect of inlet orifice on saturated CHF and flow visualization in multi-microchannel heat sinks, SEMI-THERM 2009. 25th Annual IEEE (2009) 1-8.
[27] B. Agostini, J.R. Thome, M. Fabbri, B. Michel, High heat flux two-phase cooling in silicon multimicrochannels, IEEE Trans Compon Packag Technol 31(3) (2008) 691-701.
[28] P. Lee, C. Pan, Boiling heat transfer and two-phase flow of water in a single shallow microchannel with a uniform or diverging cross section, J Micromech Microeng, 18(2) (2008) 025005.
[29] H.J. Lee, Y. Dong, S. Yao, Flow instability of evaporative microchannels, Int J Heat Mass Transfer 53(9–10) (2010) 1740–1749.
[30] C. Lu, C. Pan, Stabilization of flow boiling in microchannel heat sinks with a diverging cross-section design. J Micromech Microeng 18(7) (2008) 075035.
[31] C. Lu, C. Pan, A highly stable microchannel heat sink for convective boiling, J Micromech Microeng 19(5) (2009) 055013.
[32] L. Zhang, E.N. Wang, K.E. Goodson, T.W. Kenny, Phase change phenomena in silicon microchannels. Int J Heat Mass Transfer 48(8) (2005) 1572-1582.
[33] A. Kosar, C.J. Kuo, Y. Peles, Boiling heat transfer in rectangular microchannels with reentrant cavities, Int J Heat Mass Transfer 48(23–24) (2005) 4867–4886.
[34] G. Liu, J.L. Xu, Y.P. Yang, W. Zhang, Active control of flow and heat transfer in silicon microchannels. J Micromech Microeng 20(4) (2010) 045006.
[35] J. Xu, G.H, Liu, W. Zhang, Q. Li, B. Wang, Seed bubbles stabilize flow and heat transfer in parallel microchannels. Int J Multiphas Flow 35(8) (2009) 773-790.
[36] Y. Han, N. Shikazono, Stabilization of flow boiling in a micro tube with air injection. *Exp Therm Fluid Sci* 35(7) (2011) 1255-1264.
[37] H.F. Tuo, P.S. Hrnjak, Periodical reverse flow and boiling fluctuations in a microchannel evaporator of an air-conditioning system. *Int J Refrig* 36(4) (2013) 1263-1275.
[38] H.F. Tuo, P.S. Hrnjak, Flash gas bypass in mobile air conditioning system with R134a. *Int J Refrig* 35(7) (2012) 1869-1877.
[39] H.F. Tuo, P.S. Hrnjak, New approach to improve performance by venting periodic reverse vapor flow in microchannel evaporator. *Int J Refrig* (2013), DOI: 10.1016/j.ijrefrig.2013.05.020.
[40] C.D. Bowers, S.S. Wujek, P.S. Hrnjak, Quantification of Refrigerant Distribution and Effectiveness in Microchannel Heat Exchangers Using Infrared Thermography. *Int Refrig and Air Conditioning Conf at Purdue* (2010) No.2117.
[41] H.F. Tuo, A. Bielskus, P.S. Hrnjak, Experimentally validated model of refrigerant distribution in a parallel microchannel evaporator. *SAE Int J Mater Manuf* 5(2) (2012) 365-374.
[42] H.F. Tuo, P.S. Hrnjak, Effect of the header pressure drop induced flow maldistribution on the microchannel evaporator performance/ *Int J Refrig* (2013), DOI: 10.1016/j.ijrefrig.2013.06.002.
[43] D. Bogojevic, K. Sefiane, G. Duursma, A.J. Walton, Bubble dynamics and flow boiling instabilities in microchannels, *Int J of Heat Mass Transfer* 58 (1-2) (2013) 663-675.

Appendix

Table 1. Summary of previous works on reverse flow and boiling instabilities

Author/Year	Fluid and ranges of G (kg/m^2s) & q (kW/m^2)	Channel shape, size (D_h), numbers C#	Fluid inlet & exit states	Reverse flow reported
Brutin et al. [1]	n-Pentane G=125-475; q=200-700	Rectangular (S), D_h=889μm	In: Subcooled, Exit: x=20%-40%	Yes
Wu and Cheng [2]	Water G = 144 – 251; q = 9.6 – 155	Trapezoidal, D_h=158.8,82.8μm #CH = 8,15	In: Subcooled Exit: No superheat	No
Hetsroni et al., [3]	Water G=95-340; q=80-330	Triangular D_h=129 μm #CH = 13,21	In: Subcooled Exit: low x (<10%)	Yes
Zhang et al. [5]	Water/HFE-7100 G = 5 – 345; q = 30-44	Rectangular D_h=100,220,337 #CH =100,40,25	In: Subcooled Exit: No superheat	No
Qu and Mudawar [10]	Water G = 134.9 – 400.1; q = 208 – 316	Rectangular D_h = 349 μm #CH = 6	In: Subcooled Exit: x<15%	Yes
Bogojevic et al. [12]	Water G = 173 - 178; q = 219 – 577	Rectangular D_h = 193.6 μm #CH = 40	In: Subcooled Exit: x<15%	No
Brutin and Tadrist [13]	n-Pentane G=95.8-2258; q=15.7-125.6	Rectangular (S), D_h=889μm	In: Subcooled; Exit: x=0-1.0	No
Hetsroni et al., [14]	Water, Ethanol G = 28.5 – 1267; q = 50.7 – 365	Triangular D_h=100,130,220 μm #CH = 13,21,26	In: Subcooled Exit low x (<8%)	Yes
Chang and Pan [15]	Water G = 22 -110; q = 7.86 – 95.5	Rectangular D_h = 86.3μm #CH = 15	In: Subcooled Exit: No superheat	Yes
Wu and Cheng [16]	Water G = 112 – 146; q = 20 – 2400	Trapezoidal, D_h=186μm #CH = 8	In: Subcooled Exit: x<16%	No
Balasubramanian and Kandlikar [17]	Water G = 112 – 120; q = 208 – 316	Rectangular D_h = 333 μm #CH = 6	In: Subcooled Exit: No superheat	Yes
Lee and Mudawar [18]	R134a G = 127 – 654; q=316 – 938	Rectangular Dh=349μm #CH = 6	In: x_{in} =0.1%-25% Exit: x_{out}=49%-superheat	No
Xu et al. [19]	Water/Methanol G = 20 -1200; q = 130 - 392	Rectangular D_h = 436 μm #CH = 26	In: Subcooled Exit: No superheat	No
Huh et al. [20]	Water G = 170 – 360 q = 200 – 530	Rectangular (S) D_h = 103.5μm	In: Subcooled Exit: No superheat	No
Kuo and Peles [21]	Water G = 86 – 520 q = 200 – 1600	Rectangular D_h = 223 μm #CH = 5	In: Subcooled Exit: No superheat	No
Barber et al. [22]	FC-72 G= 32; q=4.26	Rectangular (S), D_h=889μm	In: Subcooled Exit: No superheat	Yes
Bogojevic et al. [23]	Water G = 72.2 – 433.3; q=178 – 445	Rectangular D_h=194μm #CH = 40	In: Subcooled Exit: No superheat	No

Table 2. Summary of methods explored to suppress boiling oscillations in microchannels

Methods	Author/Year	Fluid and ranges of G (kg/m^{2}s) & q (kW/m^2)	Channel shape, size (D_h), numbers #CH)	Main features
Inlet restrictors or orifices	Qu and Mudawar [10]	Water G = 134.9 – 400.1; q = 208 – 316	Rectangular D_h = 349 μm #CH = 6	Upstream throttling valve
	Kosar et al. [24]	Water G=115–389; q=90–6140	Rectangular, D_h=227μm #CH = 5	Four inlet orifices with different length and width
	Kandlikar et al. [25]	Water G = 120; q = 298 – 308	Rectangular, D_h=333μm #CH = 6	51% and 4% of MC cross-sectional area
	Jung Eung et al. [26]	R134a, R236fa, R245fa G = 200 – 2000; q = 0 – 1800	Rectangular, D_h=837,315μm #CH = 20,29	Two orifices: Circular (300 μm); Rectangular (200×765 μm)
	Agostini et al. [27]	R236fa G = 30 – 1880; q = 250 – 2200	Rectangular D_h = 122 μm #CH = 134	Rectangular orifices (500×67 μm)
Expanding channels	Lee and Pan [28]	Water G = 209 – 625; q = 117 –361	Rectangular D_h = 33.3 μm #CH = 1	Diverging angle of 0.183°
	Lee et al. [29]	Water G = 48.5; q=22 – 23.5	Rectangular D_h=353μm #CH = 48	Double channel area at downstream by combining two channels
	Lu and Pan [30]	Water G = 99 –297; q = 238 – 246	Rectangular D_h = 120 μm #CH = 10	Diverging angle of 0.5°
	Lu and Pan [31]	Water G=198; q=241 – 244	Triangular D_h=120 μm #CH = 10	Diverging angle of 0.5° + 25 cavities (20-22 μm)
Artificial nucleation cavities	Kuo and Peles [21]	Water G = 86 – 520 q = 0 – 210	Rectangular D_h = 223 μm #CH = 5	Nonconnected and interconnected reentrant cavities on the sidewalls
	Kandlikar et al. [25]	Water G = 120; q = 298 – 308	Rectangular, D_h=333μm #CH = 6	Artificial nucleation sites (5 – 30 μm)
	Zhang et al. [32]	Water m = 0.02 ml/min; Q = 0 – 2.7 W	Rectangular D_h=27–171	Notches(4 μm, on side wall) + cavities (4-8 μm, on the bottom)
	Kosar et al. [33]	Water G = 41 – 302; q=280 – 4450	Rectangular D_h=227μm #CH = 5	7.5 μm wide reentrant cavities on the sidewalls
Seed bubble	Liu et al. [34]	Methanol G = 100 – 1100; q = 0 – 374	Triangular D_h=100 μm #CH = 5	Seed bubble created by microheater at f = 10, 100, 1000 Hz
	Xu et al. [35]	Acetone G = 377.9 – 897.6; q = 439 – 939.9	Rectangular D_h = 100 μm #CH = 5	Seed bubble created by microheater at f = 10, 100, 1000 Hz
	Han and Shikazono [36]	Water G = 169 – 254 q = 72 – 584	Rectangular (S) D_h = 497μm	Air injection with varied flow rates

MIXED CONVECTIVE HEAT TRANSFER IN TRANSITIONAL AND TURBULENT FLOWS

Oosthuizen P.H.
Department of Mechanical and Materials Engineering,
Queen's University,
Kingston, Ontario
Canada K7L 3N6
E-mail: oosthuiz@queensu.ca

ABSTRACT

In situations in which there is a forced flow over a body that has a surface temperature that is different from the temperature of the undisturbed flow upstream of the body the buoyancy forces that arise due to the density differences associated with the temperature differences in the flow can have a significant effect on the flow over the body and consequently on the heat transfer rate from the body. Such flows, in which there is a forced velocity but in which the buoyancy force effects are important, are termed mixed- or combined natural and forced convective flows. Most, but certainly not all, past studies of mixed convection have been concerned with situations involving laminar flow. However, in many practical situations in which mixed convection exists the flow can be transitional or fully turbulent. The flows that occur in such situations can be quite complex because the presence of the buoyancy forces not only affects the momentum balance but also affects the turbulent flow structure. In this paper mixed convective flow over a thin vertical flat plate for conditions under which transition from laminar to turbulent flow occurs will be considered. Attention will be given both to the case where the buoyancy forces act in the same direction as the forced flow, i.e., to the case of assisting mixed convective flow, and to the case where the buoyancy forces act in the opposite direction to the forced flow, i.e., to the case of opposing mixed convective flow. Consideration will also be given to the so-called laminarization phenomena. Results for both the case where the plate is maintained at a uniform surface temperature and where there is a uniform heat flux over the surface of the plate are discussed. A relatively brief discussion of mixed convective flow over flat plates that are inclined to the vertical and of mixed convective flow over cylinders is also presented. Attention has lastly be given an example of a practical situations that can involve mixed convection the example considered being one that arises in heat transfer to or from a building window system.

INTRODUCTION

When there is a forced flow over a body that has a surface temperature that is different from the temperature of the undisturbed forced flow the buoyancy forces that arise due to the density differences associated with the differences in the flow can have a significant effect on the flow and consequently on the heat transfer rate from the body. Flows such as these, see Fig. 1, are termed mixed- or combined natural and forced convective flows.

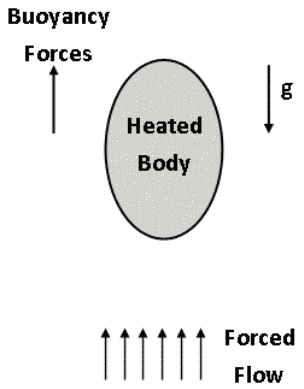

Figure 1 Mixed or combined natural and forced convective flow

The majority of past studies of mixed convection have been concerned with situations involving laminar flow but many practical situations in which mixed convection occurs involve turbulent flows. Turbulent mixed convective flows can be quite complex because the presence of the buoyancy forces not only effects the momentum balance but also effects the turbulent flow structure. The purpose of this paper is to review some recent studies of mixed convective flows that consider conditions under which laminar flow, transitional flow, and turbulent flow exist.

The main attention in this paper will be given to mixed convective flow over a thin flat plate. The forced flow is, in all cases, parallel to the surface of the plate. One example of this type of flow is shown in Fig. 2.

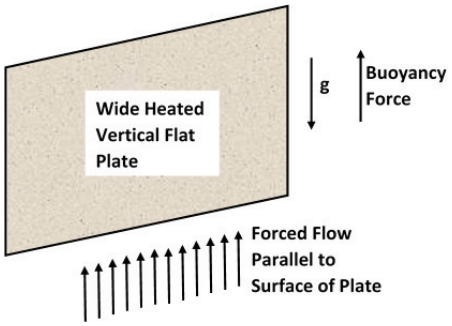

Figure 2 Mixed convective flow over a thin vertical isothermal plate

The heat transfer rate in such situations depends on the thermal boundary conditions at the surface of the plate and the angle of the plate and the therefore of the forced flow relative to the direction of the buoyancy forces. Two surface thermal boundary conditions will be considered in the discussion given here, one of these being where the plate surface is at a uniform temperature, i.e., is isothermal, and the other being where there is a uniform rate of heat transfer over the plate surface. In general, the plate can be at any angle to buoyancy forces. Two particular cases (see Fig. 3 which shows flows over an arbitrary shaped body) have received the most attention, these being the case where the buoyancy forces act in the same direction as the forced flow, i.e., the case of assisting or aiding mixed convective flow, and the case where the buoyancy forces act in the opposite direction to the forced flow, i.e., the case of opposing mixed convective flow. Both will be considered here. However, some attention will also be given to the case where the plate is inclined at an arbitrary angle to the vertical.

In many studies of mixed convection the main aim of the work has been to determine the conditions under which mixed convective flow exists and thus to determine the conditions under which the effects of the buoyancy forces are negligible, i.e., to determine when purely forced convection effectively exists and to determine the conditions under which the effects of the forced flow are negligible, i.e., to determine when purely natural convection effectively exists.

In addition to discussing mixed convective flows over flat plates brief consideration will here also be given to mixed convective flows over cylinders. Attention will also lastly be given to a practical situation that involves mixed convection, the example chosen being that of flow from a hot-air floor mounted vent over a cold window covered by a blind system.

As mentioned before there have been many studies of laminar mixed convection from vertical flat plates typical of these being those described in [1-19]. A number of studies of turbulent and transitional mixed convection are available. Among these are [20-35]. Studies of the reduction in the heat transfer rate that can occur in turbulent mixed convection, this phenomena often being termed laminarization, are described in [36-38] for example. Unsteady and complex flows can develop in mixed convection, this being discussed, for example, in [39-44]. However, this will not be discussed to any significant extent in the present paper. Previous studies of mixed convection that were concerned in some way with turbulent flows have concentrated mainly on the local Nusselt number variation. Here, attention will be given to only the mean Nusselt number variation. The discussion presented in this paper is mainly based on the results presented in [45–52].

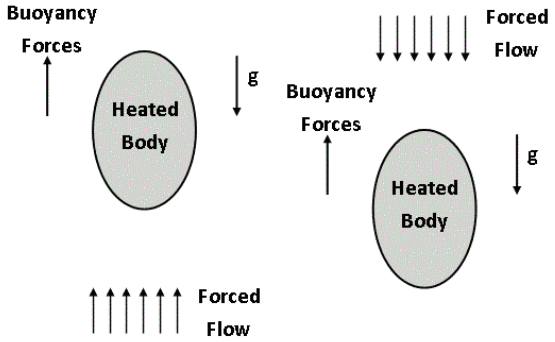

Figure 3 Assisting or aiding mixed convective flow (left) and opposing mixed convective flow (right)

FLAT PLATE FLOW NUMERICAL SOLUTION PROCEDURE

Most of the results discussed in this paper were derived numerically and most are concerned with flow over a flat plate. In the numerical study of flows such as that shown in Fig. 2 it has been assumed that the flow is steady and two-dimensional. Fluid properties have been assumed constant except for the density change with temperature which gives rise to the buoyancy forces. This was treated using the so-called Boussinesq approach, i.e., it has been assumed that the fluid properties are constant except for the density change with temperature which gives rise to the buoyancy forces and that the density change is linearly dependent on the temperature change.

Most of the solutions discussed here have been obtained by numerically solving the governing equations mainly using the commercial CFD solver ANSYS FLUENT©. The *k*-epsilon turbulence model was used with full account being taken of buoyancy force effects. This turbulence model is applied under all conditions and determines whether laminar, transitional, or turbulent flow exists. This turbulence model has, in past studies, e.g. see [53-55], been found to give relatively good predictions of when transition to turbulence occurs and of the flow and heat transfer in the laminar, transitional and turbulent flow regions.

PRESENTING THE RESULTS

In the case of flow over a flat plate the mean heat transfer rate from the surface of the plate has been expressed in terms of the mean Nusselt number based on the plate length, *L*, defined as follows:

$$Nu = \frac{q'L}{\left(T_m - T_f\right)k} \tag{1}$$

where q' is the mean heat flux over the plate surface and T_m and T_f are the mean plate temperature and the temperature of the undisturbed fluid far from the plate respectively.

The solution has the following parameters:

1. The Rayleigh number, *Ra* (uniform surface temperature) or *Ra** (uniform surface heat flux), based on the plate length, *L*, and the mean temperature difference or the uniform surface heat flux, i.e.:

$$Ra = \frac{\beta g\left(T_w - T_f\right)L^3}{\nu^2}Pr \quad \text{or} \quad Ra^* = \frac{\beta g q' L^4}{\nu^2 k}Pr \tag{2}$$

2. The Reynolds number, *Re*, based on the length of the plate and on the velocity in the undisturbed forced flow ahead of the plate, *U*:

$$Re = \frac{U L}{\nu} \tag{3}$$

3. The Prandtl number, *Pr*
4. The angle of the plate to the vertical, φ

In the studies discussed here it has been assumed that air flow is involved and that *Pr* is constant and equal to 0.74. Since a single value of *Pr* is being considered for the isothermal plate case:

$$Nu = \text{function}\left(Re, Ra, \varphi\right) \tag{4}$$

while for the uniform surface heat flux case:

$$Nu = \text{function}\left(Re, Ra^*, \varphi\right) \tag{5}$$

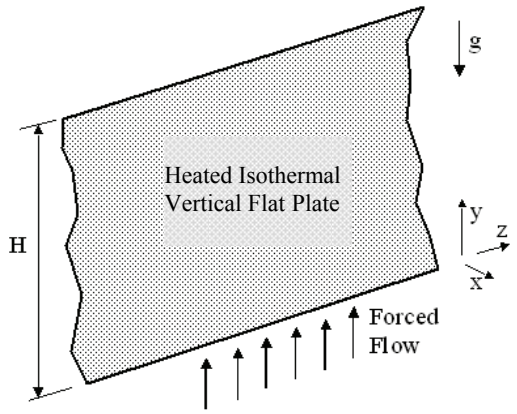

Figure 4 Assisting mixed convective flow over a thin vertical isothermal plate [45]
(Oosthuizen PH (2010) IHTC14-22448. By permission ASME)

LAMINAR AND TURBULENT ASSISTING MIXED CONVECTIVE FLOW OVER A VERTICAL ISOTHERMAL PLATE

Attention will first be given to the case of assisting mixed convective flow over a vertical isothermal plate. If the plate is heated, i.e., is at a surface temperature that is higher than the temperature of the ambient fluid far from the plate surface, assisting flow will occur when the forced flow is in the vertically upward direction as shown in Fig. 4.

The variations of mean Nusselt number with Reynolds number for various decreasing Rayleigh numbers are shown in the following Figs. 5, 6, and 7. Figure 5 shows results for the highest Rayleigh number considered (10^{11}) and Figures 6 and 7 show results for two lower Rayleigh numbers.

Consideration will first be given to the results for the highest three Rayleigh numbers.

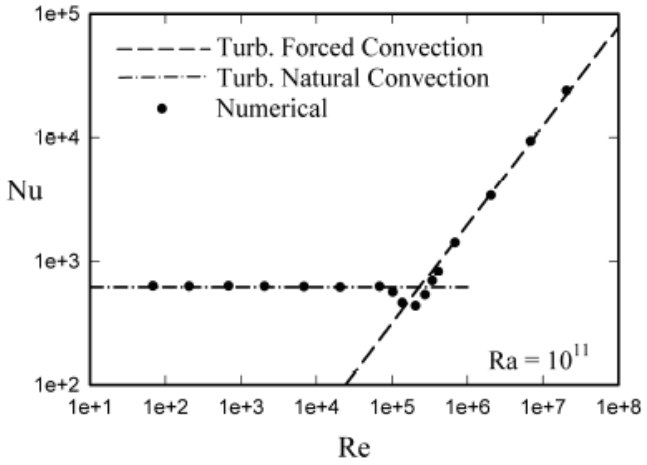

Figure 5 Variation of mean Nusselt number with Reynolds number for $Ra = 10^{11}$ [45]
(Oosthuizen PH (2010) IHTC14-22448. By permission ASME)

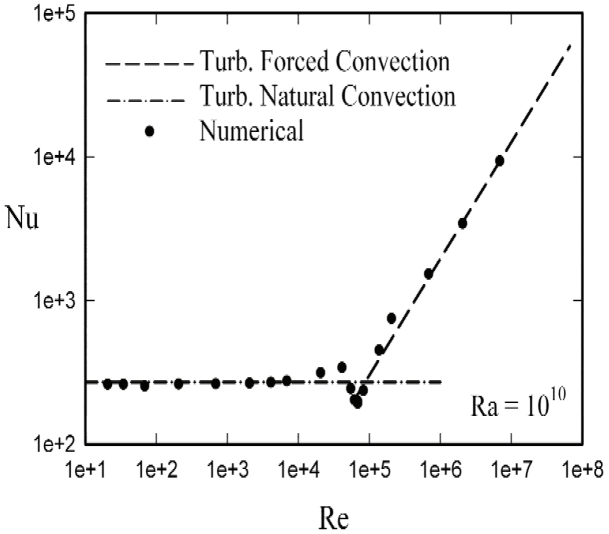

Figure 6 Variation of mean Nusselt number with Reynolds number for $Ra = 10^{10}$ [45]
(Oosthuizen PH (2010) IHTC14-22448. By permission ASME)

The three Rayleigh numbers for which results are given in the above figures are high enough to expect that in all cases the flow will be turbulent. The Nusselt numbers will be seen in the

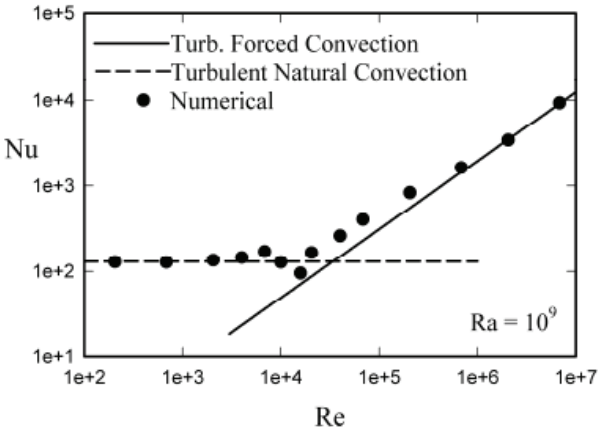

Figure 7 Variation of mean Nusselt number with Reynolds number for $Ra = 10^9$ [45]
(Oosthuizen PH (2010) IHTC14-22448. By permission ASME)

above figures to pass from those that apply in turbulent natural convection at the lower Reynolds number values to those that apply in turbulent forced convection at the higher Reynolds number values. Between these two limits the Nusselt number will be seen to pass through a minimum. This is often said to be due to laminarization, i.e., to a decrease in the intensity of the turbulence resulting from the effects of the buoyancy forces on the turbulence structure. The form of the variation is shown in Fig. 8.

The variation of the minimum Nusselt number, Nu_{min}, with Rayleigh number obtained from these and other similar results is shown in Fig. 9 and the variation of the Reynolds number, Re_{min} , (see Fig. 8) at which the minimum Nusselt number occurs with Rayleigh number obtained from these results is shown in Figure 10.

Attention will next be turned to the results for some of the lower Rayleigh numbers considered. Typical results are shown in Figs. 11, 12, and 13.

In all cases it will be seen from Figs. 11, 12, and 13 that the flow changes through the mixed convection region from either turbulent or laminar (depending on the Rayleigh number value) natural convection to turbulent forced convection.

The results obtained in the study described above indicate that:

1. The *k-ε* turbulence model adequately predicts the conditions under which transition from laminar to turbulent flow occurs in the limiting conditions of purely natural convection and purely forced convection. It also appears to give adequate predictions of the conditions under which transition occurs in mixed convection.
2. At the higher Rayleigh number values considered (above approximately 10^9) the flow is turbulent under all conditions considered. Under these conditions, as the Reynolds number at a given Rayleigh number is increased, the mean Nusselt number passes through a minimum. The presence of this minimum is associated with laminarization.

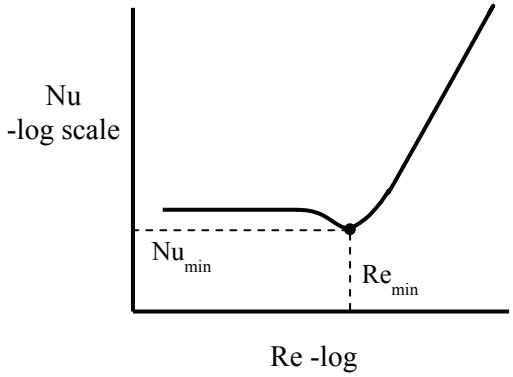

Figure 8 General form of variation of mean Nusselt number with Reynolds number

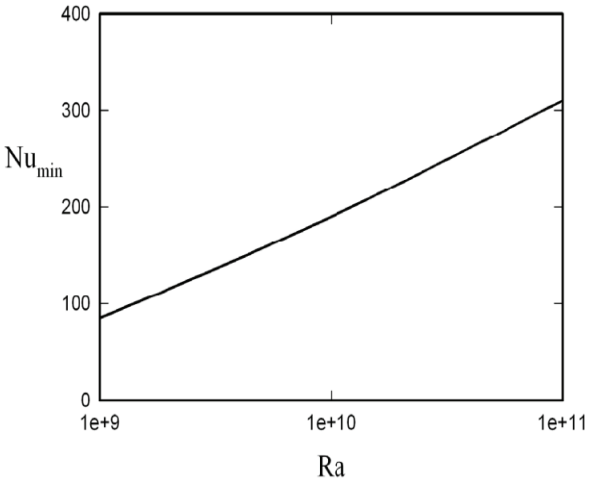

Figure 9 Variation of minimum mean Nusselt number with Rayleigh number [45]
(Oosthuizen PH (2010) IHTC14-22448. By permission ASME)

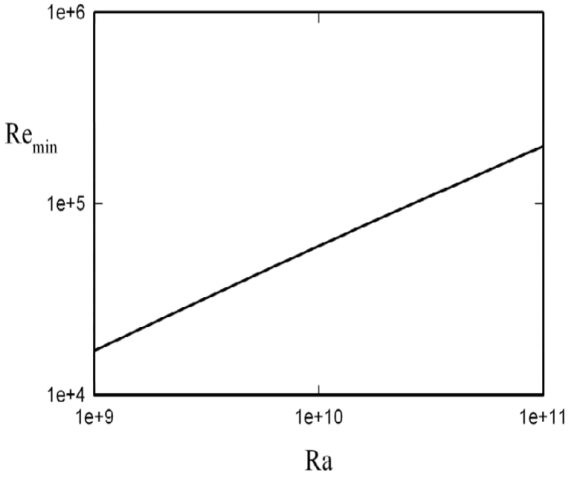

Figure 10 Variation of Reynolds number at which the minimum mean Nusselt number occurs with Rayleigh number [45]
(Oosthuizen PH (2010) IHTC14-22448. By permission ASME)

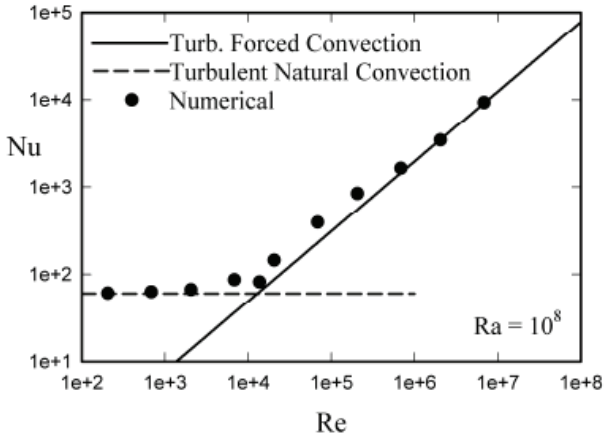

Figure 11 Variation of mean Nusselt number with Reynolds number for $Ra = 10^8$ [45]
(Oosthuizen PH (2010) IHTC14-22448. By permission ASME)

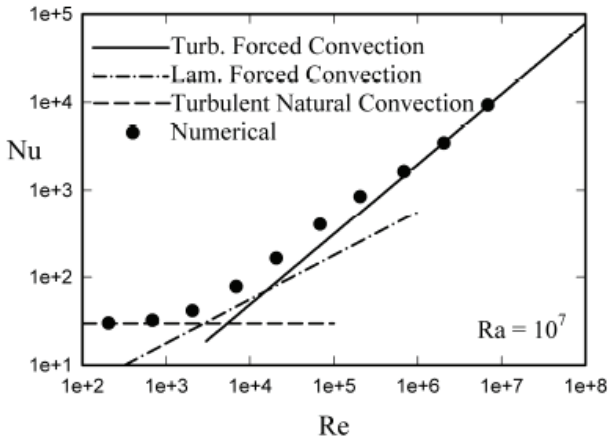

Figure 12 Variation of mean Nusselt number with Reynolds number for $Ra = 10^7$ [45]
(Oosthuizen PH (2010) IHTC14-22448. By permission ASME)

3. At the lower values of Rayleigh number considered, as the Reynolds number increases, the mean Nusselt numbers first becomes essentially equal to the values that would exist in laminar forced convection and then at higher Reynolds numbers become essentially equal to the values that would exist in turbulent forced convection.

PREDICTION OF LAMINARIZATION

The results given in the previous section showed that at the higher Rayleigh and Reynolds numbers the variation of Nusselt number with Reynolds number for a fixed Rayleigh number passed through a minimum in the mixed convection region. This is often said to be the result of laminarization, i.e., the result of the "dampening" of the intensity of the turbulence by the buoyancy forces. The classical mixing-length approach indicates, for example, that in mixed convective flow the eddy viscosity is given by [38]:

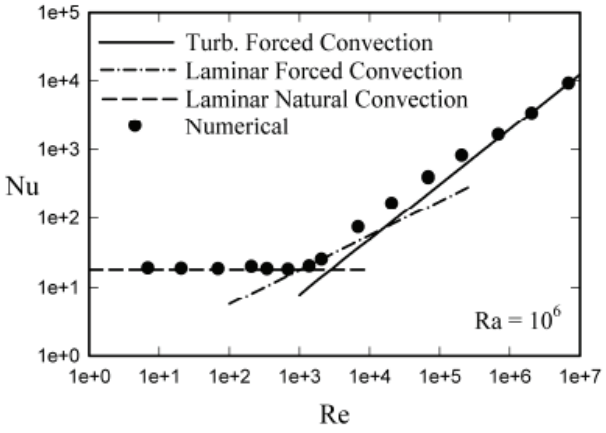

Figure 13 Variation of mean Nusselt number with Reynolds number for $Ra = 10^6$ [45]
(Oosthuizen PH (2010) IHTC14-22448. By permission ASME)

$$\varepsilon = \frac{\tau}{\rho\left(\frac{\partial u}{\partial y}\right)} = \ell^2 \left|\frac{\partial u}{\partial y}\right| \left| 1 + J\beta g \frac{\left(\frac{\partial T}{\partial y}\right)}{\left(\frac{\partial u}{\partial y}\left|\frac{\partial u}{\partial y}\right|\right)} \right| \tag{6}$$

where y is the coordinate normal to the surface and J is a constant. The mixing length approach also indicates that the turbulent Prandtl number, Pr_T, is a constant. This equation shows that if flow over a heated wall is considered, since $\partial u / \partial y$ is positive near the wall and $\partial T / \partial y$ is negative, the buoyancy forces produce a decrease in the eddy viscosity and consequently a decrease in the heat transfer rate.

LAMINAR AND TURBULENT ASSISTING MIXED CONVECTIVE FLOW OVER A VERTICAL PLATE WITH A UNIFORM SURFACE HEAT FLUX

The discussion above was concerned with mixed convective flows over plates that had a uniform surface temperature. Now, the thermal boundary conditions at the plate surface can be expected to influence the nature of the flow over the plate. To investigate whether this is, in fact, the case attention in this section will be given to flow over a heated vertical plate when there is a uniform surface heat flux over the surface of the plate which heats the plate surface to a higher temperature than the temperature of the undisturbed fluid flow. The flow situation considered is thus as shown in Fig. 14.

The numerical results presented here were obtained using the same procedure as that used in dealing with the isothermal plate case. Results have again only been obtained for $Pr = 0.74$, i.e., essentially the value for air.

Variations of the mean Nusselt number with Reynolds number for various increasing values of the heat flux Rayleigh number are shown in the Figs. 15, 16, 17, and 18. It will be seen from the variations shown in Figs. 15 to 18 that in all cases the mean Nusselt numbers pass from those that apply in purely natural convection at the lower Reynolds number values

to those that apply in turbulent purely forced convection at the higher Reynolds number values.

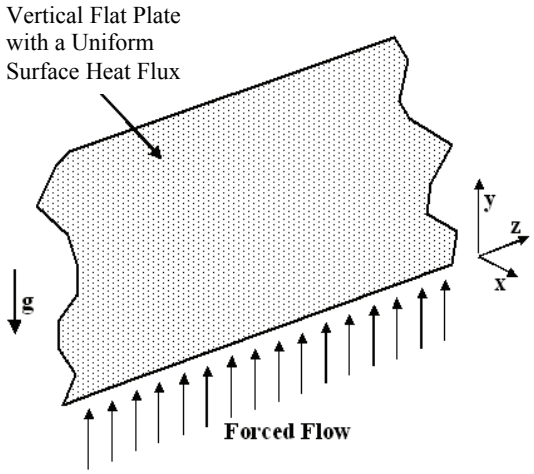

Figure 14 Assisting mixed convective flow over a thin vertical plate with a uniform surface heat flux [46]

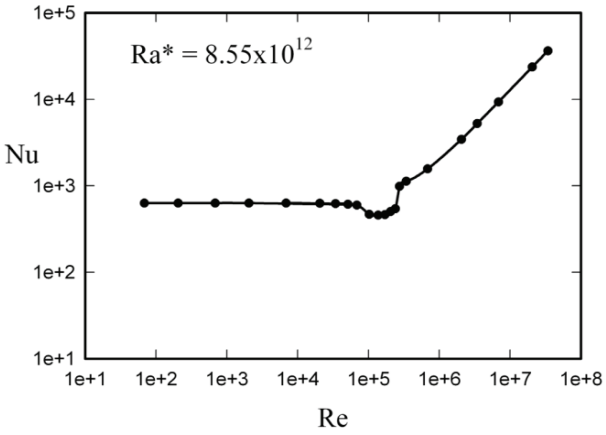

Figure 15 Variation of Mean Nusselt number with Reynolds number for a heat flux Rayleigh number, Ra^* of 8.55×10^{12} [46]

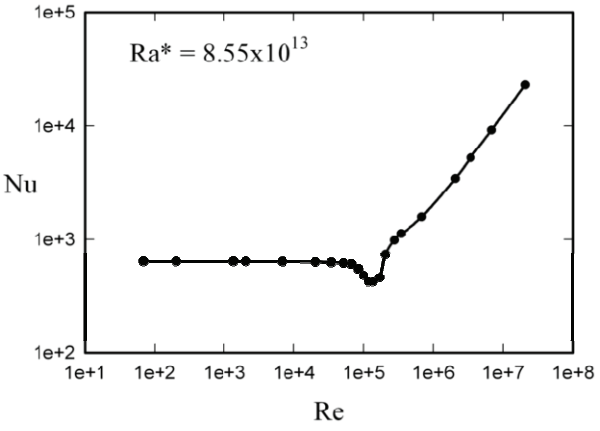

Figure 16 Variation of Mean Nusselt Number with Reynolds Number for a heat flux Rayleigh number, Ra^* of 8.55×10^{13} [46]

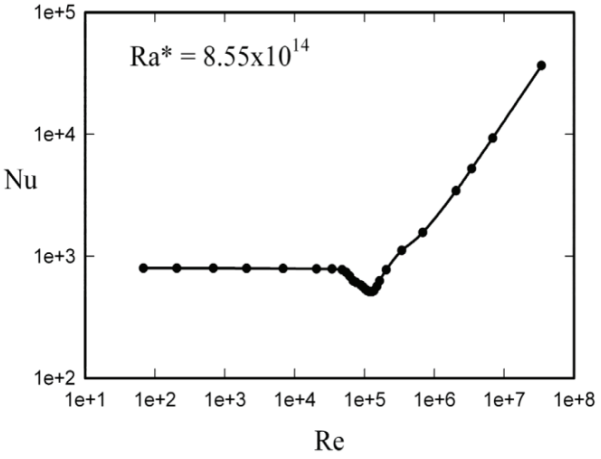

Figure 17 Variation of Mean Nusselt number with Reynolds number for a heat flux Rayleigh number, Ra^*, of 8.55×10^{14} [46]

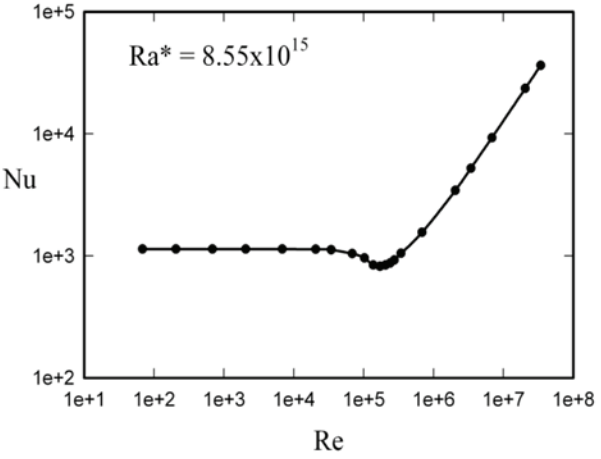

Figure 18 Variation of mean Nusselt number with Reynolds number for a heat flux Rayleigh number, Ra^*, of 8.55×10^{15} [46]

The general form of the variation is shown in Fig. 19. Between these two limits the Nusselt number will again be seen to pass through a minimum. The basic form of the variation of the mean Nusselt number with Reynolds number is thus similar to that which occurs with assisting mixed convective flow over a vertical isothermal plate.

The variation of the minimum value of the Nusselt number, Nu_{min}, with the heat flux Rayleigh number is shown in Fig. 20.

It will be seen that the lowest Nusselt number value, Nu_{min}, decreases with increasing Ra^* up to values of about 2×10^{14} and then increases with further increase in Ra^*. Now, numerical studies of purely natural convective flow over a vertical flat plate with a uniform surface heat flux indicate that fully turbulent flow is reached approximately when Ra^* has a value of 7×10^{14}. Therefore, the minimum in the variation of Nu_{min} with Ra^* occurs near the Ra^* value at which the natural convective flow reaches a fully turbulent state.

In an attempt to correlate results for mixed convective flows it has often been assumed that:

$$\frac{Nu}{Nu_{nat}} = \text{function}\left(\frac{Nu_{for}}{Nu_{nat}}\right) \tag{7}$$

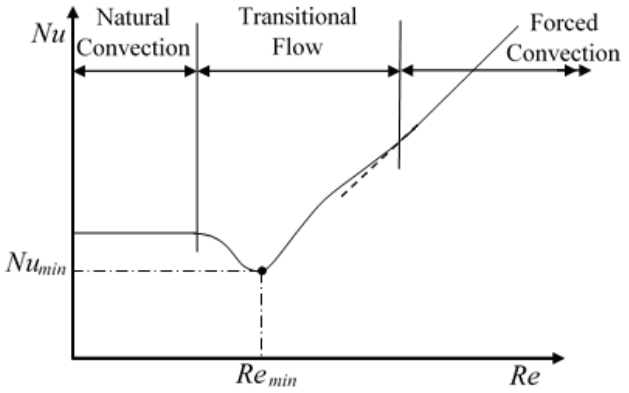

Figure 19 General form of the variation of mean Nusselt number with Reynolds number for a given heat flux Rayleigh number [46]

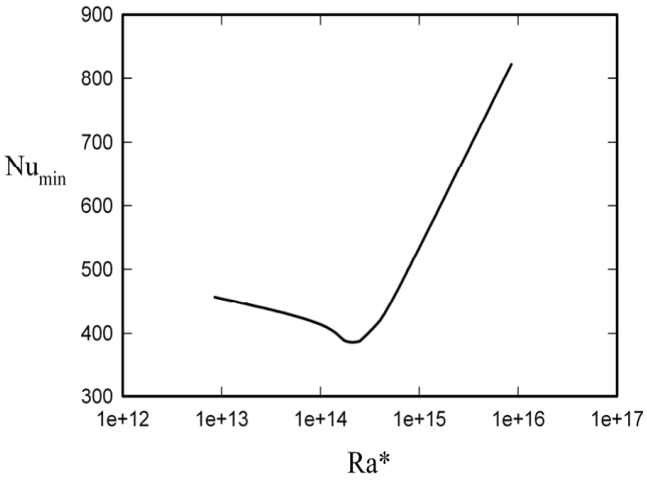

Figure 20 Variation of the minimum value of the Nusselt number, Nu_{min} , with the heat flux Rayleigh number [46]

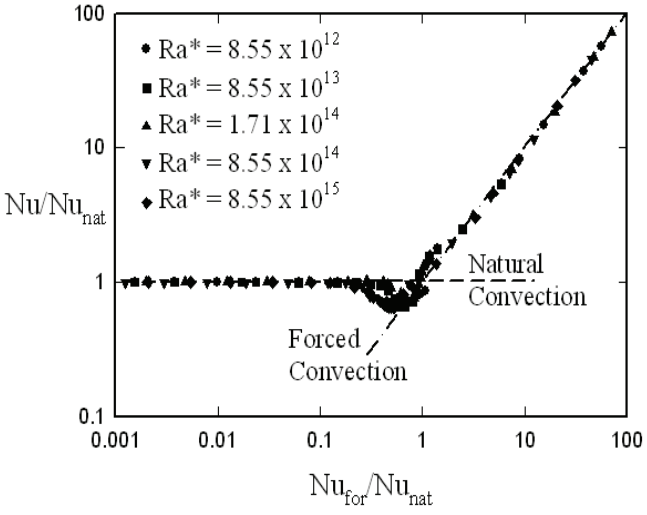

Figure 21 Variation of the minimum value of Nu / Nu_{nat} with Nu_{for} / Nu_{nat} for a range of values of the heat flux Rayleigh numbers [46]

where Nu_{nat} is the Nusselt number that would exist under the same conditions as being considered, i.e. at the same values of Ra^* and Pr, in purely natural convective flow and Nu_{for} is the Nusselt number that would exist under the same conditions as being considered, i.e. at the same values of Re and Pr, in purely forced convective flow. The results obtained have been plotted in this way in Fig. 21.

While the results when plotted in this way are somewhat scattered in the vicinity of the point at which the minimum Nusselt number occurs it will be seen from the above figure that the results do indicate the following approximate results:

$$\text{Purely Natural Convective Flow when : } \frac{Nu_{for}}{Nu_{nat}} \text{ is less than 0.2}$$

$$\text{Purely Forced Convective Flow when : } \frac{Nu_{for}}{Nu_{nat}} \text{ is greater than 2}$$

$$\text{Minimum Nusselt Number when: } \frac{Nu_{for}}{Nu_{nat}} = 0.7$$

$$\text{Minimum Nusselt Number value given by: } Nu_{\min} = 0.75 Nu_{nat}$$

A similar approach can be used in dealing with the isothermal plate case.

LAMINAR, TRANSITIONAL, AND TURBULENT OPPOSING MIXED CONVECTIVE FLOW OVER A VERTICAL ISOTHERMAL PLATE

In the previous two sections attention was given to mixed convective flow over a thin vertical plate for the case where the buoyancy forces act in the same direction as the forced flow, i.e., to assisting flow over a vertical plate. In the present section attention will be given to flow over a thin isothermal vertical flat plate for the case where the buoyancy forces act in the opposite direction to the forced flow, i.e., to opposing flow over a vertical isothermal plate. The flow situation considered in this section is thus as shown in Fig. 22. The results presented in this section were obtained in [50]. In the next section attention will be given to opposing mixed convection over a thin vertical plate for the case where the there is a uniform heat flux over the surface of the plate.

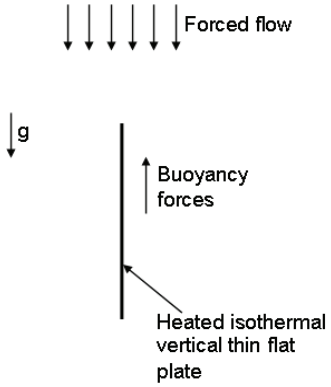

Figure 22 Opposing mixed convective flow over a thin vertical isothermal flat plate [50] (Reprinted by permission of the American Institute of Aeronautics and Astronautics, Inc.)

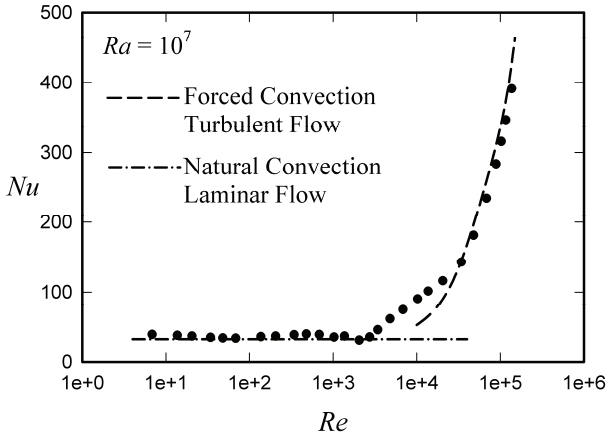

Figure 23 Variation of mean Nusselt number with Reynolds number for opposing mixed convective flow over a vertical isothermal plate for a Rayleigh number of 10^7 [50] (Reprinted by permission of the American Institute of Aeronautics and Astronautics, Inc.)

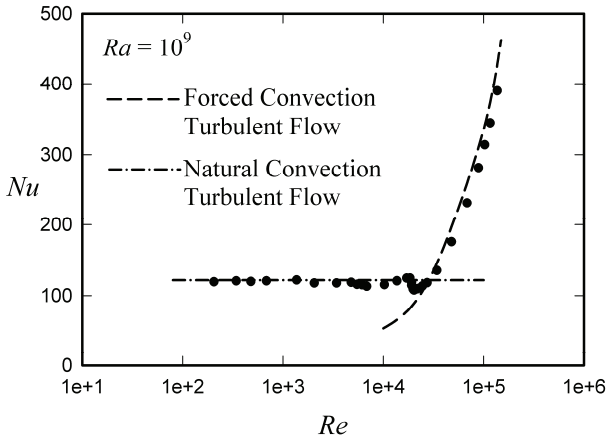

Figure 24 Variation of mean Nusselt number with Reynolds number for opposing mixed convective flow over a vertical isothermal plate for a Rayleigh number of 10^9 [50] (Reprinted by permission of the American Institute of Aeronautics and Astronautics, Inc.)

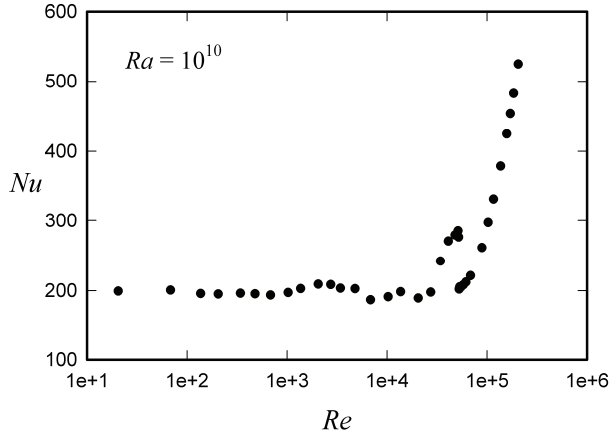

Figure 25 Variation of mean Nusselt number with Reynolds number for opposing mixed convective flow over a vertical isothermal plate for a Rayleigh number of 10^{10} [50] (Reprinted by permission of the American Institute of Aeronautics and Astronautics, Inc.)

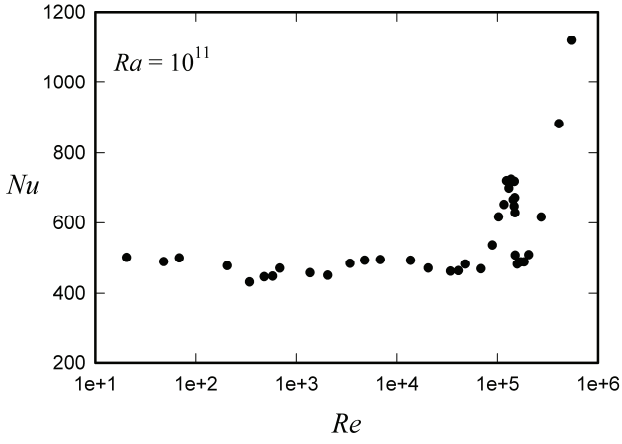

Figure 26 Variation of mean Nusselt number with Reynolds number for opposing mixed convective flow over a vertical isothermal plate for a Rayleigh number of 10^{11} [50] (Reprinted by permission of the American Institute of Aeronautics and Astronautics, Inc.)

Results have again only been obtained for $Pr = 0.74$, i.e., essentially for the value of Pr for air. Ra values between approximately 10^7 and 10^{11} and Re values between approximately 10^3 and 10^6 have been considered. Because under certain conditions non-symmetrical flow develops in the situation here being considered the heat transfer rates from the two sides of the plate are, in general, different. However, here attention will only be given to the mean heat transfer rate averaged over the two sides of the plate.

Results covering flows ranging between purely natural convective flow, through mixed convective flow to purely forced convective flow have been obtained. Typical variations of the mean Nusselt number with Reynolds number for Rayleigh numbers of 10^7, 10^9, 10^{10}, and 10^{11} for this situation are shown in Figs. 23, 24, 25, and 26.

It will be seen from Figs. 23 to 26 that in all cases at low Reynolds numbers the Nusselt numbers are essentially equal to the purely natural convective value corresponding to the value of the Rayleigh number being considered while at high Reynolds numbers the Nusselt numbers are equal to the purely forced convective values at the Reynolds number value being considered. Between these two limiting conditions mixed convective flow exists.

When transitional and turbulent flow conditions exist in the mixed convective flow region the Nusselt number variation in this mixed convective flow region becomes complex because the flow in this region is generally not symmetrical about the vertical plane containing the plate, i.e., the flow is different over the two sides of the plate. Another important reason for the complex flow in the mixed convection region is associated with the effects of the buoyancy forces on the turbulence.

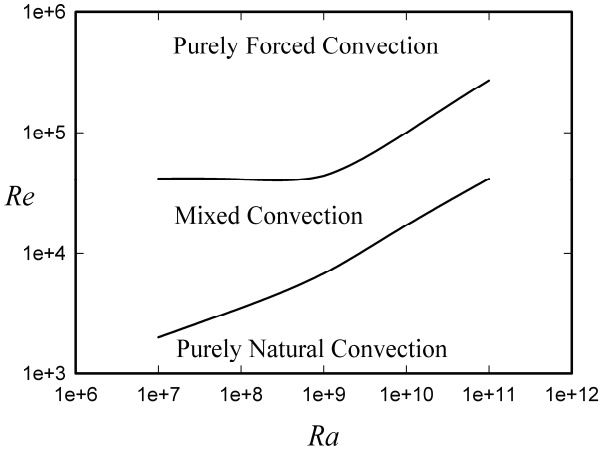

Figure 27 Variation of Reynolds number with Rayleigh number that define when purely forced convection, when purely natural convection, and when mixed convection can be assumed to exist [50] (Reprinted by permission of the American Institute of Aeronautics and Astronautics, Inc.)

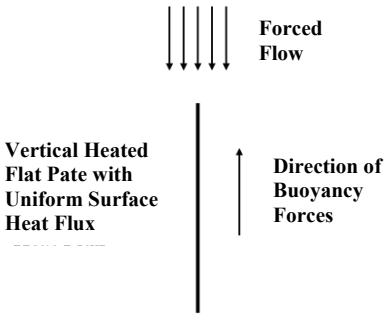

Figure 28 Flow situation considered [47] (Oosthuizen PH (2014), HEFAT, Begell House Inc.)

The main interest in the study here being discussed was to determine the conditions under which the flow can be assumed to be purely natural convection and under which it can be assumed to be purely forced convection, i.e., to determine the conditions under which mixed convective flow exists. The values of the Reynolds number below which the flow can be assumed to be purely natural convective and above which the flow can be assumed to be purely forced convective for a particular Rayleigh number can be determined from results such as those shown in the preceding figures. Using the results so obtained the variations of Reynolds number with Rayleigh number that define when purely forced convection and when purely natural convection can be assumed to exist can be derived and is shown Fig. 27.

There is quite a large uncertainty in these curves due to the unsymmetrical flow that can exist in the transition regions between purely natural and mixed convective flows and between purely forced and mixed convective flows.

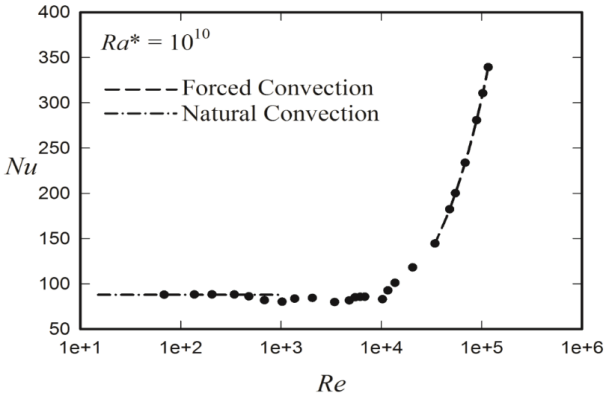

Figure 29 Variation of mean Nusselt number with Reynolds number for opposing mixed convective flow over a vertical plate with a uniform surface heat flux for a heat flux Rayleigh number of 10^{10} [47] (Oosthuizen PH (2014), HEFAT, Begell House Inc.)

The results of the study being considered here indicate that:

1. In the mixed convective flow region and in the transitional flow region the flow is generally not symmetrical about the vertical plane containing the plate, i.e., the flow is different over the two sides of the plate.
2. At the higher Rayleigh numbers considered complex variations of Nusselt number with Reynolds number exist.
3. The figure given above can be used to define the variation of Reynolds number with Rayleigh number that determines approximately when purely forced convection can be assumed to exist and to define the variation that determines when purely natural convection can be assumed to exist.

LAMINAR, TRANSITIONAL, AND TURBULENT OPPOSING MIXED CONVECTIVE FLOW OVER A VERTICAL PLATE WITH A UNIFORM SURFACE HEAT FLUX

In this section brief consideration will be given to opposing mixed convective flow over a vertical plate for the case where there is a uniform surface heat flux over the plate surface. The situation considered is as shown in Fig. 28.

Results have again only been obtained for $Pr = 0.74$, i.e., essentially for the value for air. Ra^* values between about 10^{10} and 10^{13} and Re values between approximately 10^2 and 10^6 have been considered.

The variations of the mean Nusselt number with Reynolds number for heat flux Rayleigh numbers of 10^{10}, 10^{11}, 10^{12}, and 10^{13} are shown in Figs. 29, 30, 31, and 32.

In all cases, as is to be expected, at low Reynolds numbers the Nusselt numbers are equal to the purely natural convective number being considered while at high Reynolds numbers the Nusselt numbers are equal to the purely forced convective values. The general form of the variation is shown in Fig. 33.

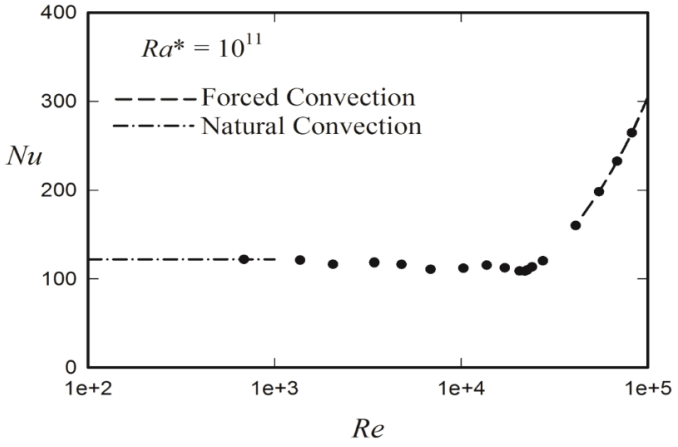

Figure 30 Variation of mean Nusselt number with Reynolds number for opposing mixed convective flow over a vertical plate with a uniform surface heat flux for a heat flux Rayleigh number of 10^{11} [47] (Oosthuizen PH (2014), HEFAT; Begell House Inc.)

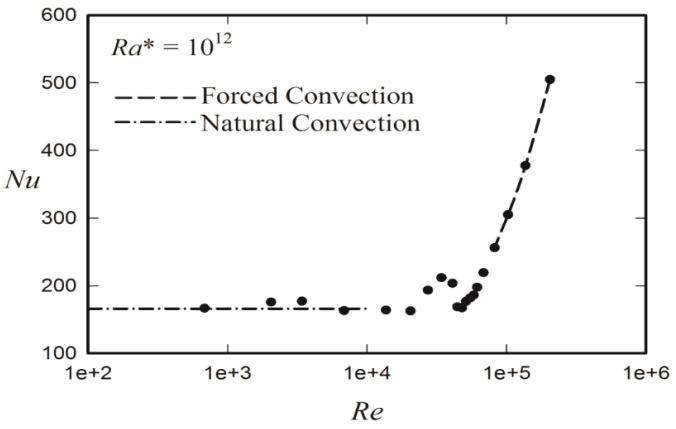

Figure 31 Variation of mean Nusselt number with Reynolds number for opposing mixed convective flow over a vertical plate with a uniform surface heat flux for a heat flux Rayleigh number of 10^{12} [47] (Oosthuizen PH (2014), HEFAT; Begell House Inc.)

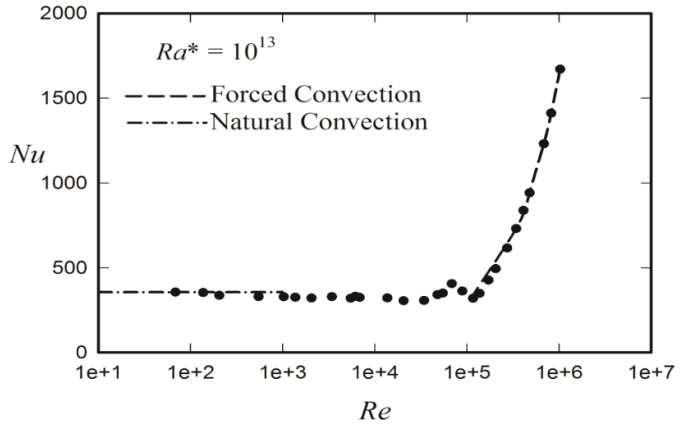

Figure 32 Variation of mean Nusselt number with Reynolds number for opposing mixed convective flow over a vertical plate with a uniform surface heat flux for a heat flux Rayleigh number of 10^{13} [47] (Oosthuizen PH (2014), HEFAT; Begell House Inc.)

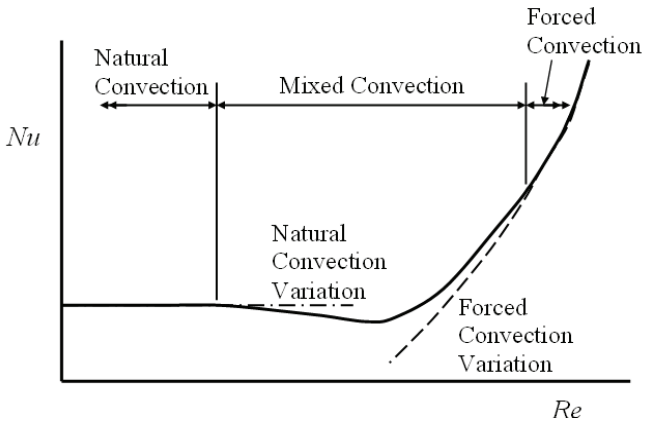

Figure 33 General form of the variation of mean Nusselt number with Reynolds number for opposing mixed convective flow over a vertical plate with a uniform surface heat flux at a given heat flux Rayleigh number [47] (Oosthuizen PH (2014), HEFAT; Begell House Inc.)

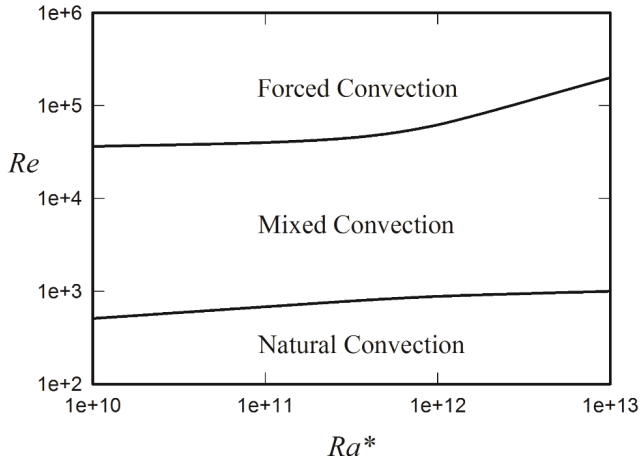

Figure 34 Variations of Reynolds number with Heat Flux Rayleigh number that define when forced flow, when mixed convective flow, and when natural convective flow can be assumed to exist [47] (Oosthuizen PH (2014), HEFAT; Begell House Inc.)

It will also be noted that the Nusselt number variation in mixed convection is complex because unsteady flow can exist in this region and the flow is generally not symmetrical about the vertical plane containing the plate, i.e., it is different over the two sides of the plate.

The main focus in this work was determining the conditions under which the flow can be assumed to be purely natural convection and under which it can be assumed to be purely forced convection. These conditions can be derived from the results given in the above figures and the variation so obtained of Reynolds number with Heat Flux Rayleigh number that defines when forced flow can be assumed to exist and when natural convective flow can be assumed to exist are shown in Fig. 34.

It will be seen from Fig. 34 that the change in the Reynolds number that defines when natural convective flow can be assumed to exist with Heat Flux Rayleigh number is relatively small. It will also be seen that the range of Reynolds numbers over which mixed convection exists at a particular value of Heat Flux Rayleigh number increases significantly with increasing Heat Flux Rayleigh number.

As mentioned before the flow in the mixed convection flow region was generally found to be unsteady and the heat transfer results for this region are the time-averaged values. The mixed convection region shown in the above figure effectively, therefore, also indicates the region in which unsteady flow was observed, the flow in the purely natural convection region and in the purely forced convection region being steady.

LAMINAR, TRANSITIONAL, AND TURBULENT MIXED CONVECTIVE HEAT TRANSFER FROM A THIN INCLINED ISOTHERMAL PLATE

In this study the effect of the buoyancy forces on the heat transfer rate for conditions under which flow transition occurs has been studied for the particular case of flow parallel to the surface of a thin flat isothermal plate that is, in general, set at an angle to the vertical has been considered. The flow situation considered is thus as shown in Fig. 35. The results presented in this section were obtained in [48].

Attention has been restricted to the case where the plate is at a higher temperature than the temperature of the undisturbed fluid flow and the buoyancy force component parallel to the plate surface is in the same direction as the forced flow, i.e., attention has been restricted to assisting mixed convective flow.

Because the plate and therefore the forced flow is inclined to the vertical the buoyancy forces act at an angle to the forced flow as indicated in the above figure. As a result, the heat transfer rate from the two sides of the plate is, as mentioned before, in general different.

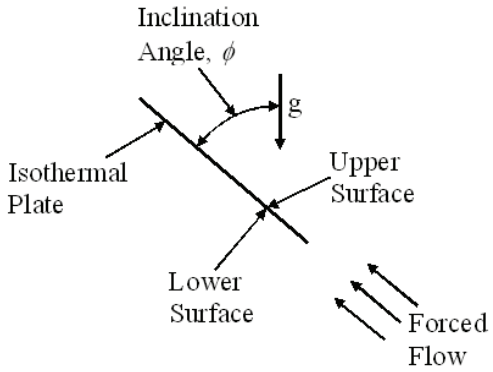

Figure 35 Flow situation considered [48]

Typical variations of the Nusselt numbers for the two sides of the plate with Reynolds number for a fixed Rayleigh number for various values of the angle of inclination are shown in Figs. 36 to 41.

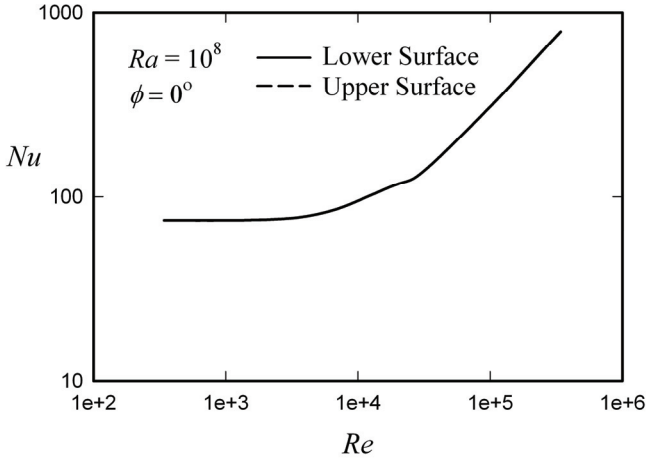

Figure 36 Variations of mean Nusselt numbers for upper and lower surfaces with Reynolds number for a Rayleigh number of 10^8 and an inclination angles of 0^o [48]

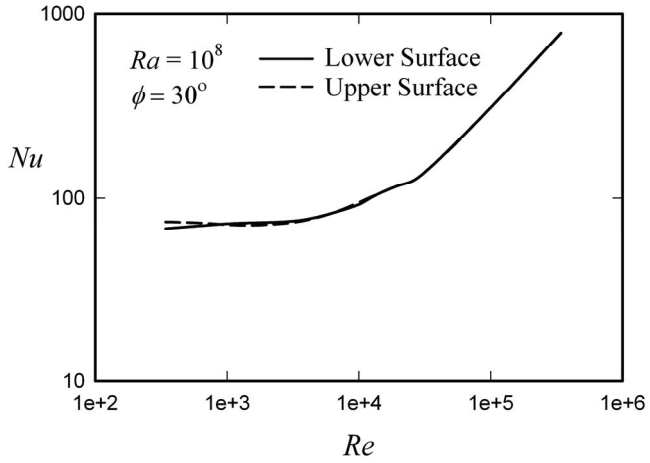

Figure 37 Variations of mean Nusselt numbers for upper and lower surfaces with Reynolds number for a Rayleigh number of 10^8 and an inclination angles of 30^o [48]

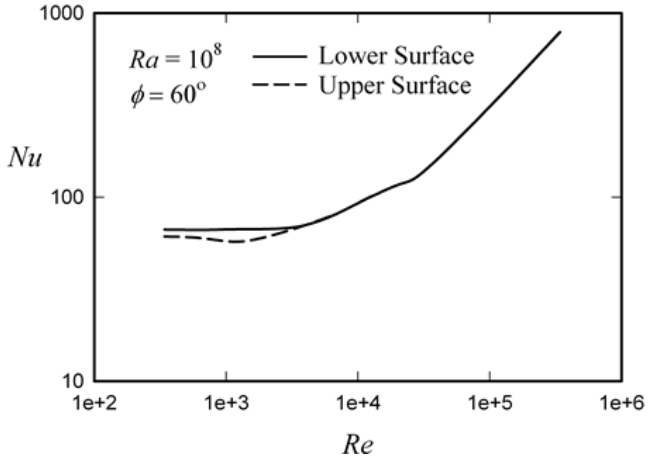

Figure 38 Variations of mean Nusselt numbers for upper and lower surfaces with Reynolds number for a Rayleigh number of 10^8 and an inclination angles of 60^o [48]

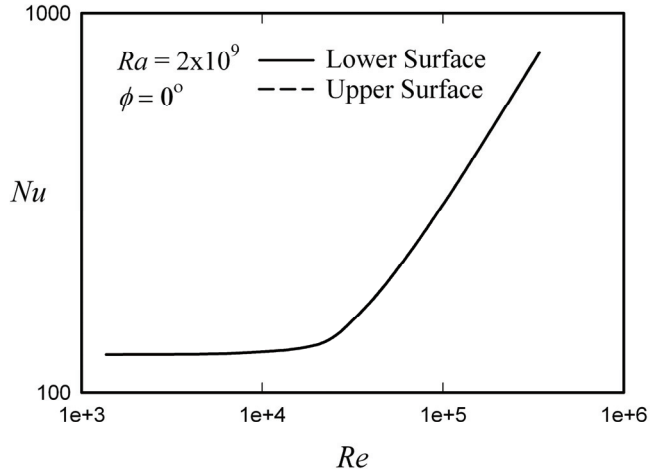

Figure 39 Variations of mean Nusselt numbers for upper and lower surfaces with Reynolds number for a Rayleigh number of $2x10^9$ and an inclination angle of 0^o [48]

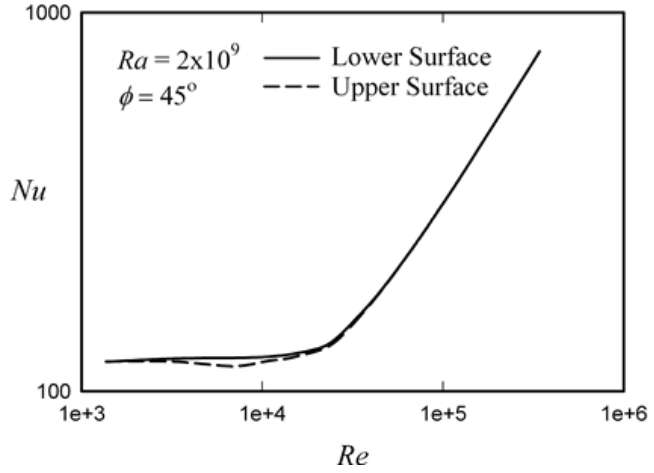

Figure 40 Variations of mean Nusselt numbers for upper and lower surfaces with Reynolds number for a Rayleigh number of $2x10^9$ and an inclination angle 45^o [48]

Figs. 36, 37, and 38 show results for a Rayleigh number of 10^8 for angles of inclination of 0^o, 30^o, and 60^o respectively while Figs. 39, 40, and 41 show results for a Rayleigh number of $2x10^9$ for angles of inclination of 0^o, 45^o, and 60^o respectively. At an angle of plate inclination of 0^o the forced flow is vertically upwards and in the same direction as the buoyancy forces and under these conditions the flow over the two sides of the plate is identical and the Nusselt numbers for the two sides of the plate therefore the same.

From these figures it will be seen that at the higher values of Reynolds number considered the buoyancy forces have a negligible effect on the Nusselt number variation with Reynolds number. Consequently the Nusselt numbers for the two sides of the plate are identical, the flow then being essentially forced convective.

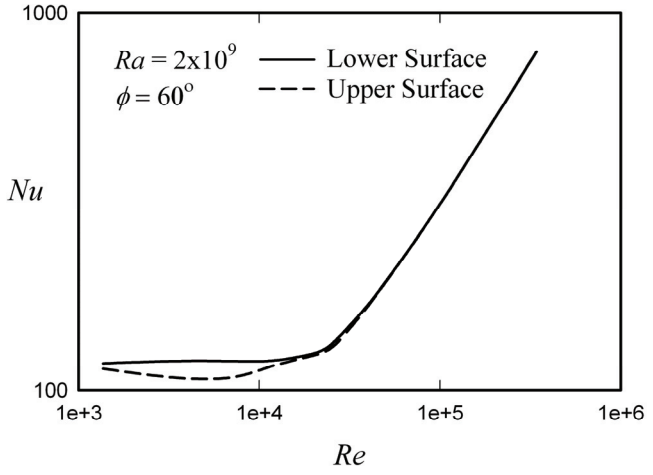

Figure 41 Variations of mean Nusselt numbers for upper and lower surfaces with Reynolds number for a Rayleigh number of $2x10^9$ and an inclination angle of 60^o [48]

At the lower Reynolds numbers considered, however, the Nusselt number becomes essentially independent of the Reynolds number, the flow then being essentially natural convective. Under these conditions the Nusselt numbers for the two sides of the plate are, in general, different, the Nusselt number for the upper surface of the plate at the higher angles of inclination considered generally being lower than the Nusselt number for the lower surface.

One of the main purposes of this work was to determine the conditions under which the flow can be assumed to be purely forced convective. In order to determine when forced flow could be assumed to exist the variations of Nusselt number with Reynolds number in mixed convective flows were compared to the variation given by the purely forced convection results, typical comparisons being shown in Figs. 42 to 47.

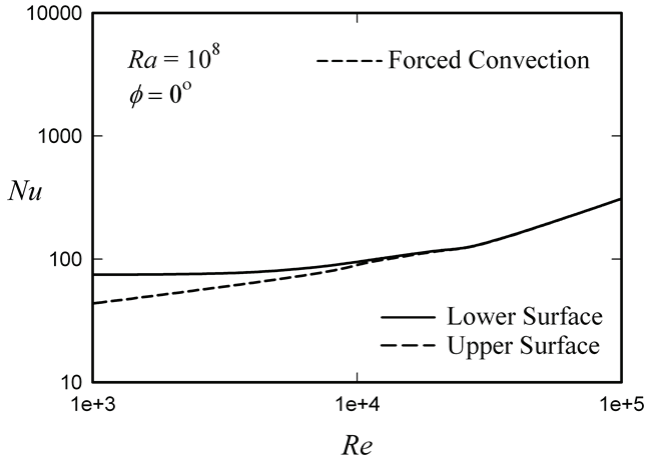

Figure 42 Comparison of variations of mean Nusselt numbers for upper and lower surfaces with Reynolds number for a Rayleigh number of 10^8 and an inclination angle of 0^o with the variation for purely forced convective flow [48]

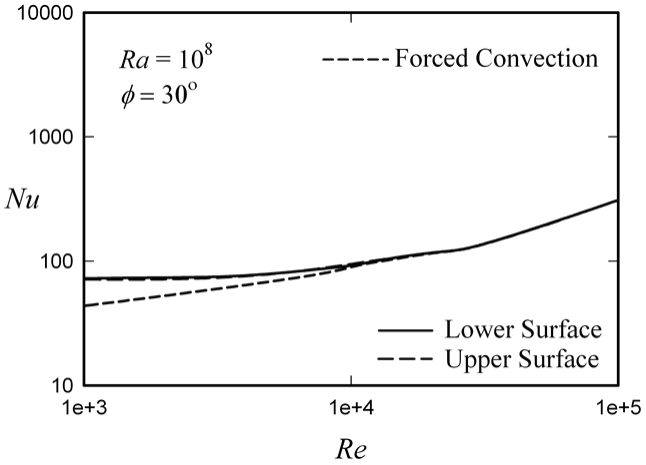

Figure 43 Comparison of variations of mean Nusselt numbers for upper and lower surfaces with Reynolds number for a Rayleigh number of 10^8 and an inclination angle of 30^o with the variation for purely forced convective flow [48]

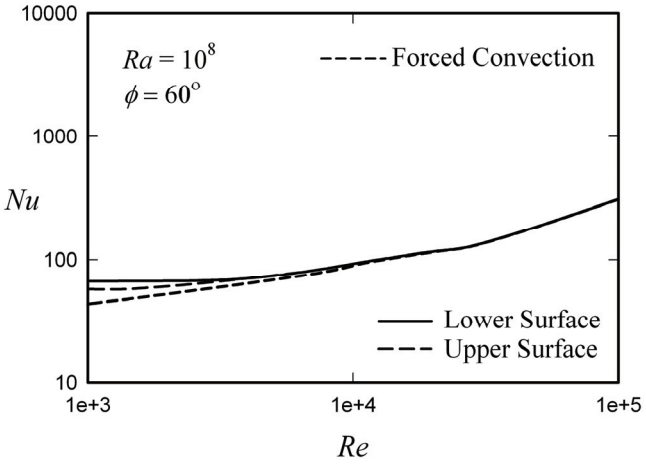

Figure 44 Comparison of variations of mean Nusselt numbers for upper and lower surfaces with Reynolds number for a Rayleigh number of 10^8 and an inclination angle of 60^o with the variation for purely forced convective flow [48]

Figures 42, 43, and 44 show results for a Rayleigh number of 10^8 for angles of inclination of 0^o, 30^o, and 60^o respectively while Figs. 45, 46, and 47 show results for a Rayleigh number of 10^{10} also for angles of inclination of 0^o, 30^o, and 60^o respectively.

It will be seen from the these figures that in all cases the deviations of the Nusselt numbers for the upper and lower surfaces of the plate from each other occurs at a lower Reynolds number than that at which the deviation of the Nusselt number curve from that for purely forced convection, i.e., the conditions under which purely forced convection can be assumed to exist are the same for the upper and lower surfaces of the plate. Using results similar to those shown in the above figures the conditions that define when forced convective flow can be assumed to exist were determined.

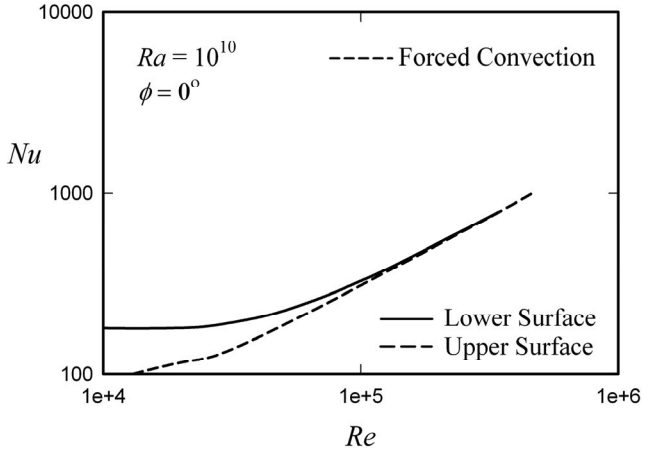

Figure 45 Comparison of variations of mean Nusselt numbers for upper and lower surfaces with Reynolds number for a Rayleigh number of 10^{10} and an inclination angle of 0^o with the variation for purely forced convective flow [48]

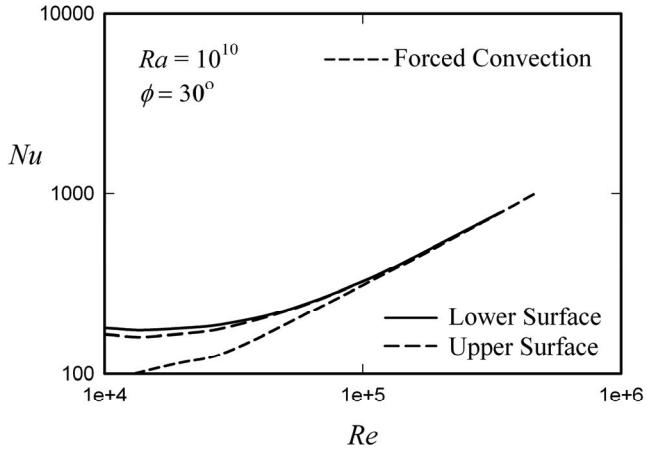

Figure 46 Comparison of variations of mean Nusselt numbers for upper and lower surfaces with Reynolds number for a Rayleigh number of 10^{10} and an inclination angle of 30^o with the variation for purely forced convective flow [48]

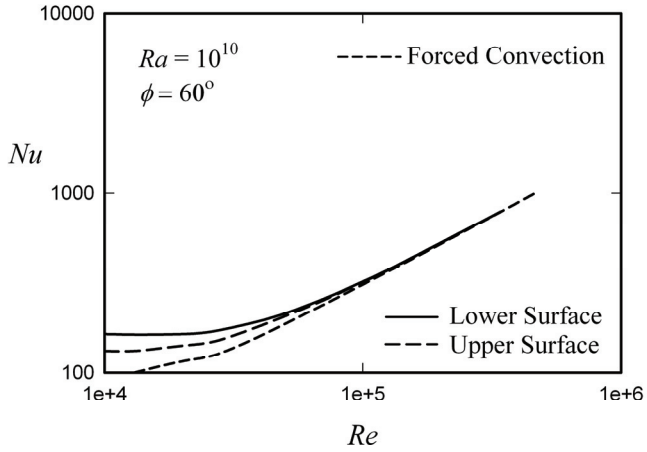

Figure 47 Comparison of variations of mean Nusselt numbers for upper and lower surfaces with Reynolds number for a Rayleigh number of 10^{10} and an inclination angle of 60^o with the variation for purely forced convective flow [48]

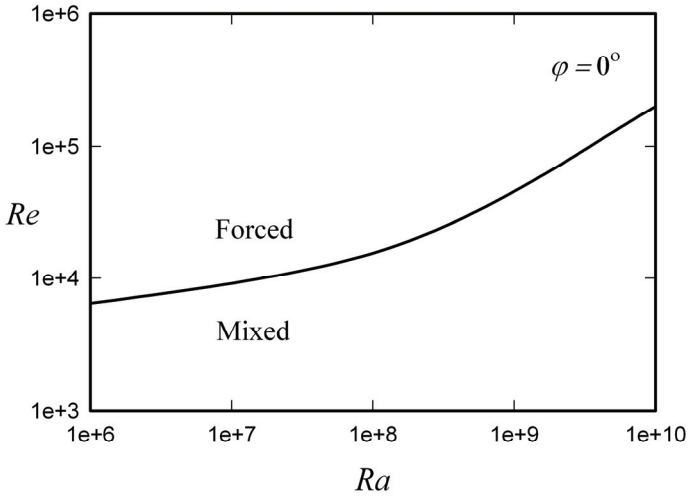

Figure 48 Reynolds number variation with Rayleigh number that define the conditions under which buoyancy force effects become significant for an inclination angle of 0^o (a vertical plate) [48]

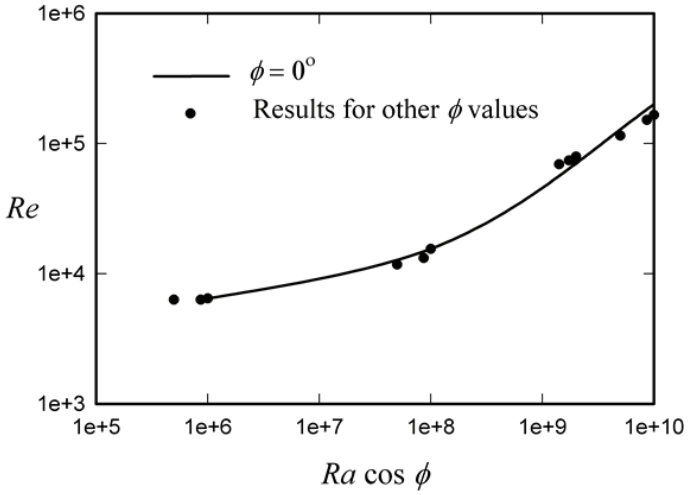

Figure 49 Reynolds number variation with $Ra\cos\varphi$ that define the conditions under which buoyancy force effects become significant for all inclination angles considered [48]

Attention will be given to results for the vertical plate case, i.e., the $\varphi = 0^o$ case. Results for this case are shown in Fig. 48. It will be seen from Fig. 48 that at the lowest Rayleigh number considered both the Reynolds number and the Rayleigh number that define the conditions under which purely forced convective flow can be assumed to exist are in the range of values under which laminar flow exists. However, at the highest Rayleigh number considered both the Reynolds number and the Rayleigh number that define the conditions under which purely forced convective flow can be assumed to exist are in the range of values under which turbulent flow exists. The results given in the above figure thus span the range of conditions from those at which laminar flow exists to those at which turbulent flow exists, i.e., the results span the transitional flow range.

Consideration will next be given to the conditions under which forced flow could be assumed to exist for the inclined plate case. It will be seen from the results given before that at a given Rayleigh number the Reynolds number at which a deviation from the purely forced convection variation first occurs decreases as the angle of inclination increases. This is because the buoyancy force component parallel to the plate surface is dependent on $g\cos\varphi$, i.e., the effective Rayleigh number is $Ra\cos\varphi$. This of course decreases with increasing φ leading to the decrease in the Reynolds number at which a deviation from the purely forced convection variation first occurs.

It is to be expected therefore that the curve that defines the conditions under which purely forced convective flow can be assumed to exist for flow over a vertical plate can be approximately applied to an inclined plate providing $Ra\cos\varphi$ is used instead of Ra. A comparison of the variation Re with $Ra\cos\varphi$ obtained from the results given for the vertical plate case with results obtained for inclined plates is shown in Fig. 49.

It will be seen that the results for a vertical plate do apply to an inclined plate provided that $Ra\cos\varphi$ is used instead of Ra. Therefore, the results given in the above figure define the conditions under which forced convective flow can be assumed to exist for both a vertical and an inclined plate.

These results indicate that:

1. Purely forced convective flow exists at the higher values of Reynolds number considered.
2. A significant difference between the Nusselt numbers for the upper and lower surfaces of the plate only exists at the higher inclination angles considered, the Nusselt numbers for the upper surface then being lower than the Nusselt numbers for the lower surface.
3. The variation of Reynolds number with Rayleigh number that determines when purely forced convection exists was first established for the vertical plate case. It was then shown that this variation will apply to the case where the plate and therefore the forced flow are at an angle to the vertical if the Rayleigh number based on the buoyancy force component parallel to the plate surface is used, i.e., provided $Ra\cos\varphi$ is used instead of Ra.

LAMINAR, TRANSITIONAL, AND TURBULENT MIXED CONVECTIVE HEAT TRANSFER FROM A THIN INCLINED PLATE HAVING A UNIFORM SURFACE HEAT FLUX

The discussion given in the previous section was concerned with flow over an inclined isothermal plate. In this section flow over an inclined plate with a uniform surface heat flux will be considered. The heat flux at the plate surface is assumed to be positive, i.e., a heated flat plate is considered. The situation considered is thus as shown Fig. 50.

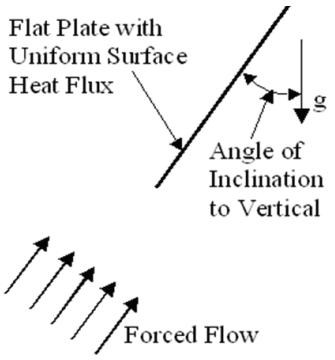

Figure 50 Flow situation considered in present section [49]
(Oosthuizen PH (2014) IHTC15-849710; Begell House Inc.)

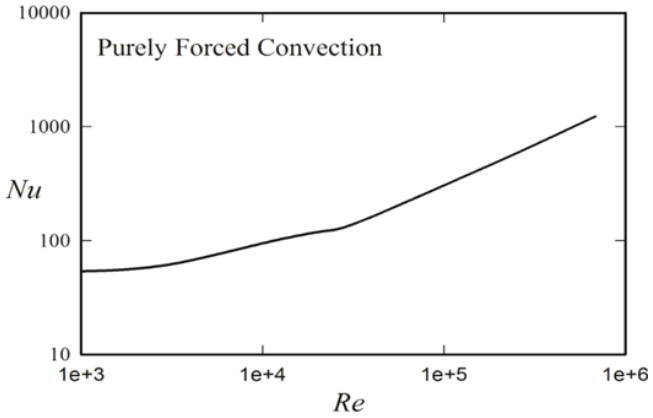

Figure 51 Variation of mean Nusselt number with Reynolds number in purely forced convective flow [49]
(Oosthuizen PH (2014) IHTC15-849710; Begell House Inc.)

Results have again only here been obtained for Pr = 0.74, i.e., essentially the value for air. Attention will first be given to the two limiting cases of purely forced convection and purely natural convection. Since results for a single value of Prandtl number are being considered in purely forced convection the Nusselt number will depend only on the Reynolds number while in purely natural convection the Nusselt number will depend on the heat flux Rayleigh number and on the angle of plate inclination to the vertical. The calculated variation of Nusselt number with Reynolds number for purely forced convection is shown in Fig. 51 and the variation of Nusselt number with heat flux Rayleigh number and angle of plate inclination to the vertical for purely natural convection is shown Fig. 52.

It will be seen that because of the range of heat flux Rayleigh numbers considered here purely natural convective flow results have only been obtained for laminar and transitional flow. Now since in purely natural convection the buoyancy force component parallel to the plate surface is expected to dominate the flow it is to be expected that the variation of Nusselt number with:

$$Ra^* \cos\varphi = \frac{\beta g q' L^4}{\nu^2 k} Pr \cos\varphi \qquad (8)$$

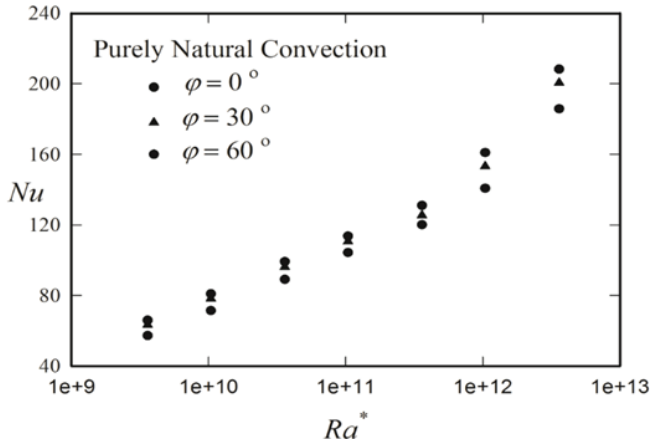

Figure 52 Variations of mean Nusselt number with heat flux Rayleigh number for various angles of plate inclination in purely natural convective flow [49]
(Oosthuizen PH (2014) IHTC15-849710; Begell House Inc.)

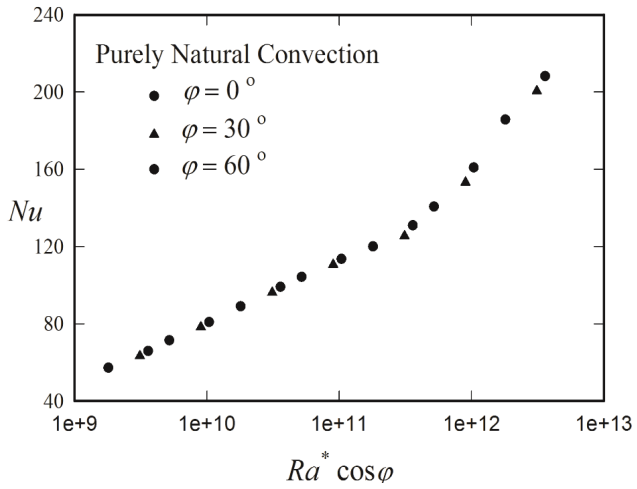

Figure 53 Correlated results for purely natural convection for various angles of plate inclination [49]
(Oosthuizen PH (2014) IHTC15-849710; Begell House Inc.)

will be independent of angle of inclination. The purely natural convection results plotted in this form are shown in Fig. 53. It will be seen from this figure that the variation of Nu with $Ra^*\cos\varphi$ is, indeed, essentially independent of the angle of inclination.

Turning next to the mixed convective flow results, Figs. 54, 55, and 56 and Figs. 57, 58, and 59 show typical variations of Nusselt number with Reynolds number for angles of plate inclination of 0°, 30°, and 60° for different values of the heat flux Rayleigh number.

It will be seen from these figures that in all cases considered the mixed convection region covers a very small range of Reynolds numbers, i.e., that as the Reynolds number decreases the Nusselt numbers go quite sharply from being equal to values in purely forced convection to being equal to the values in purely natural convection. It will also seen that no significant laminarization effects occur this being due to the fact that the

highest heat flux Rayleigh number considered is 10^{12} which is lower than that at which this effect occurs for the conditions considered here.

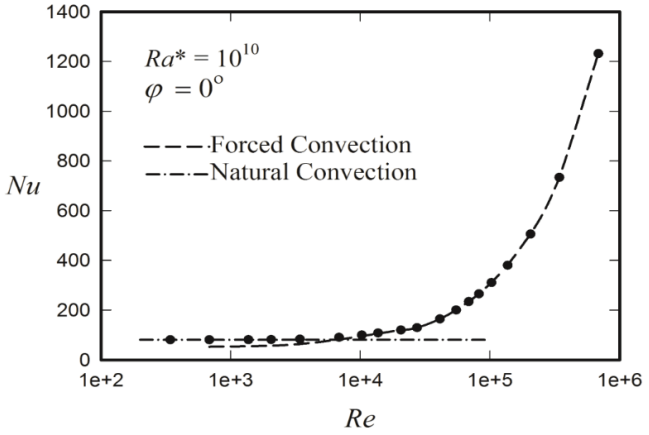

Figure 54 Variation of mean Nusselt number with Reynolds number for a heat flux Rayleigh number of 10^{10} and a plate inclination angle of 0^o[49]
(Oosthuizen PH (2014) IHTC15-849710; Begell House Inc.)

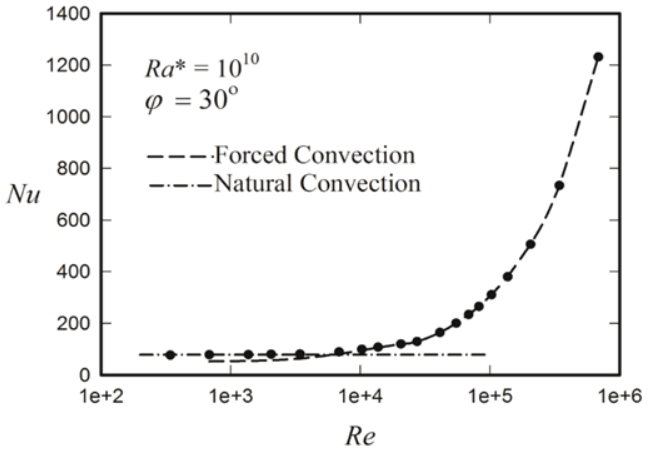

Figure 55 Variation of mean Nusselt number with Reynolds number for a heat flux Rayleigh number of 10^{10} and a plate inclination angle of 30^o [49]
(Oosthuizen PH (2014) IHTC15-849710; Begell House Inc.)

As discussed before it is common to assume that in the mixed convection region the Nusselt number is given by an equation of the form:

$$Nu^n = Nu_{for}^n + Nu_{nat}^n \text{, i.e., } \frac{Nu}{Nu_{nat}} = \left[1 + \left(\frac{Nu_{for}}{Nu_{nat}}\right)^n\right]^{\frac{1}{n}} \quad (9)$$

This equation indicates, as discussed before, that in the mixed convection region:

$$\frac{Nu}{Nu_{nat}} = \text{function}\left(\frac{Nu_{for}}{Nu_{nat}}\right) \quad (10)$$

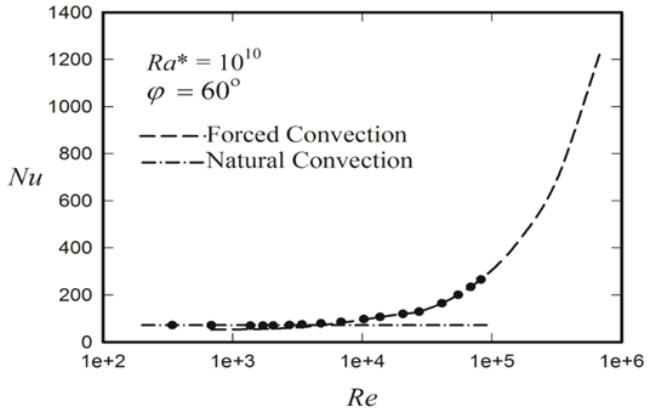

Figure 56 Variation of mean Nusselt number with Reynolds number for a heat flux Rayleigh number of 10^{10} and a plate inclination angle of 60^o [49]
(Oosthuizen PH (2014) IHTC15-849710; Begell House Inc.)

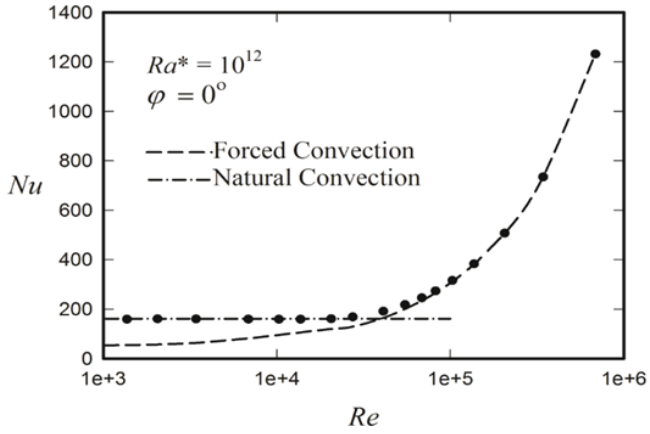

Figure 57 Variation of mean Nusselt number with Reynolds number for a heat flux Rayleigh number of 10^{12} and a plate inclination angle of 0^o [49]
(Oosthuizen PH (2014) IHTC15-849710; Begell House Inc.)

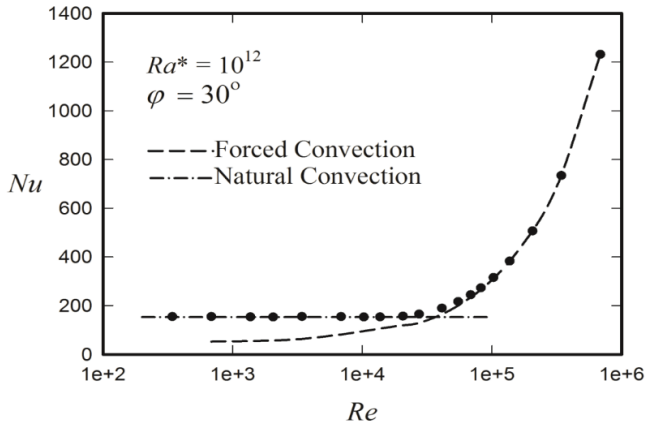

Figure 58 Variation of mean Nusselt number with Reynolds number for a heat flux Rayleigh number of 10^{12} and a plate inclination angle of 30^o [49]
(Oosthuizen PH (2014) IHTC15-849710; Begell House Inc.)

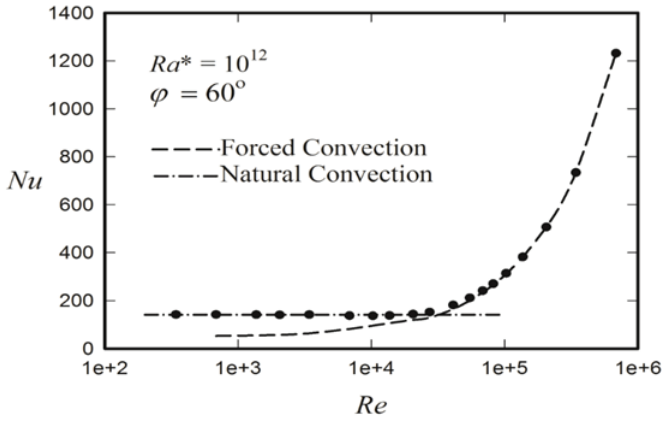

Figure 59 Variation of mean Nusselt number with Reynolds number for a heat flux Rayleigh number of 10^{12} and a plate inclination angle of 60^o [49]
(Oosthuizen PH (2014) IHTC15-849710; Begell House Inc.)

where Nu_{for} and Nu_{nat} are, as before, the Nusselt number values that would exist in purely forced convection and in purely natural convection at a particular set of values of Re, Ra^* and φ .

The variation of Nu / Nu_{nat} with Nu_{for} / Nu_{nat} for all values of Re, Ra^* and φ considered in this study is therefore shown in Fig. 60.

It will therefore be seen that an equation of this form does apply and that the results can be described to with approximately 3% by:

$$Nu^6 = Nu_{for}^6 + Nu_{nat}^6 \tag{11}$$

Using this equation or directly using the results given in Fig. 60 shows that that mixed convection exits if:

$$0.6 < \frac{Nu_{for}}{Nu_{nat}} < 1.6 \tag{12}$$

MIXED CONVECTIVE FLOW OVER HORIZONTAL CYLINDERS

The discussion given above was concerned with mixed convective flow over flat plates. A very brief discussion of mixed convective flow over horizontal circular cylinders will be presented in this section. Flow patterns over cylinders under various flow conditions are shown in Fig. 61. The reason for giving attention to this subject is that flow separation generally occurs in flow over a cylinder. In mixed convective flows the buoyancy forces influence where flow separation occurs and this has a significant effect on the convective heat transfer rate from the cylinder.

In general the flow over the cylinder will be at an angle to the vertical. However the two limiting cases of assisting and opposing flow are usually given special attention. As mentioned above one of the major effects of the buoyancy forces in mixed convective flow over a cylinder is to move the point at which flow separation occurs, e.g. see Fig. 62.

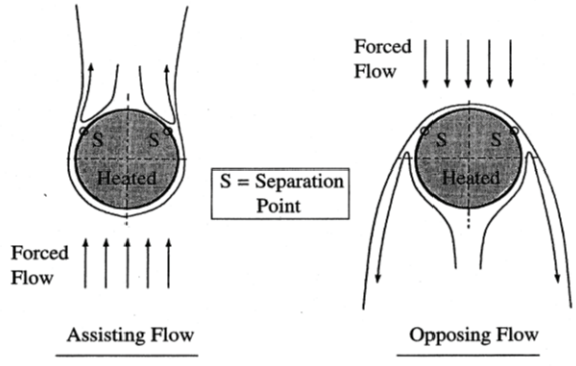

Figure 61 Flow over a horizontal cylinder placed in a horizontal forced flow with purely forced convection, purely natural convection, and mixed (combined) convection [51]

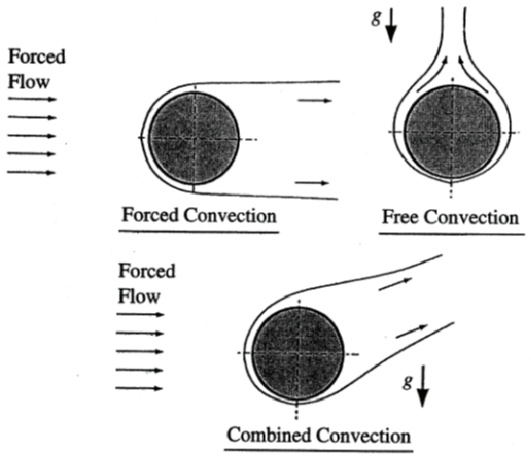

Figure 62 Separation point under the same conditions in assisting and opposing flow [51]

MIXED CONVECTION IN A "REAL WORLD" SITUATION

While the situations discussed before all do have significant practical applications it appeared to be appropriate to discuss an actual practical situation in which mixed convective flow can exist. Although the applications that can involve mixed convective flow that are most commonly mentioned are those involving the cooling of electronic and electrical equipment there are a number of flows that occur in building heat transfer that can involve mixed convective flow. One such example involves the interaction of the natural convection flow over a window and the forced flow from a below-window air vent [52]. This will be discussed here.

Air vents are often mounted below windows for various reasons including ensuring that the room occupants are afforded thermal comfort. In general, the presence of an air vent below a window changes the air flow pattern near the window and alters the rate of convective heat transfer from the window. The effect of the vent flow on the window heat

transfer rate will depend on whether or not the window is covered by a blind system. If the window is covered by a blind system, the type of blind system and the blind opening will influence the effect of the vent flow on the window heat transfer rate. The situation considered here is the particular case of a top-down, bottom-up plane blind system. Top-down, bottom-up plane blinds, that can be both raised at the bottom and lowered at the top, have become quite popular in recent times.

Such blinds may potentially reduce energy consumption in buildings since they permit the controlled use of sunlight for building illumination (daylighting) and/or the use passive solar room heating while still shading from direct sunlight and providing the room occupants with privacy. The effects of such blind systems on the convective heat transfer rate from the window to the room are considered here, the basic purpose being to determine how the vent discharge velocity affects the convective heat transfer rate from the window. Winter conditions have been considered when hot air is discharged from the floor-mounted vent and when the window is at a lower temperature than the air in the room away from the wall. The actual situation considered is only a very approximate model of most real situations (see Fig. 63).

Some typical window Nusselt number variations are shown in Figs. 64 and 65. From these figures it will be seen that the flow over the window is mainly in the mixed convection region.

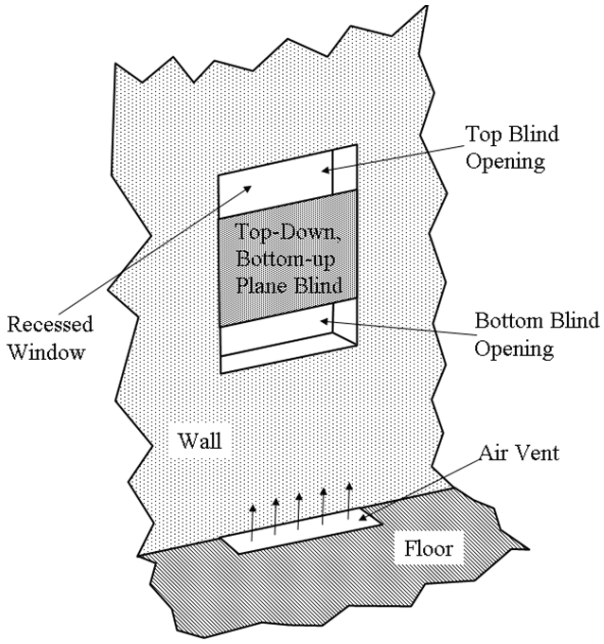

Figure 63 Flow situation considered [52] (Oosthuizen PH (2013) ASME Paper HT2013-17165. By permission)

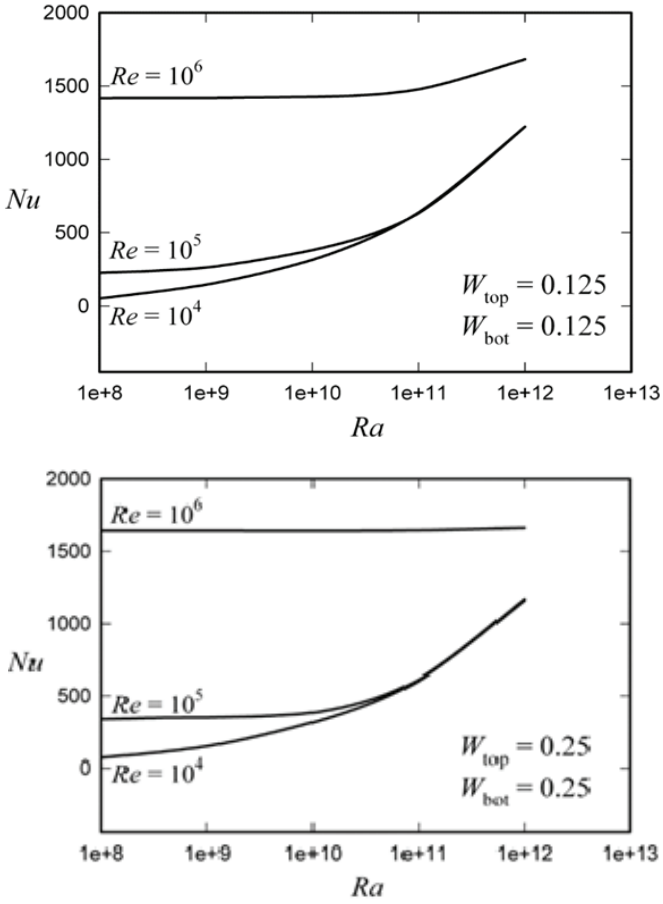

Figure 64 Variations of mean Nusselt number for the window with Rayleigh number for three Reynolds number values for the case where the dimensionless top and bottom blind openings are both 0.125 (top) and where they are 0.25 (bottom) [52] (Oosthuizen PH (2013) ASME Paper HT2013-17165. By permission)

CONCLUDING REMARKS

Although mixed convective flows have been studied for many years more work in this area is still required. Some examples of topics that require more study are:

1. Development of unsteady mixed convection flow in situations involving a forced flow at an angle to the buoyancy forces and situations involving opposing flow.
2. Further studies of laminarization in situations involving flow over bodies of more complex shape.
3. More detailed studies of the complex mixed convective flows that can arise in some building ventilation and heating or cooling situations, e.g., when hybrid ventilation systems are being used.

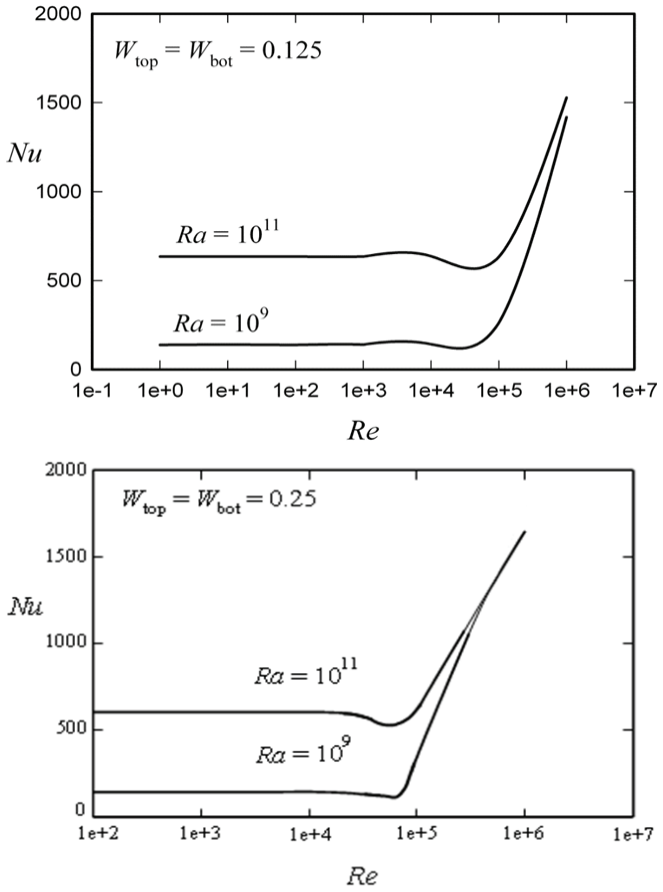

Figure 65 Variation of the mean Nusselt number for the window with Reynolds number for two Rayleigh number values for the case where the dimensionless top and bottom blind openings are both 0.125 (top) and for the case where the dimensionless top and bottom blind openings are both 0.25 (bottom) [52]
(Oosthuizen PH (2013) ASME Paper HT2013-17165. By permission)

ACKNOWLEDGEMENTS

This work was supported by the Natural Sciences and Engineering Research Council of Canada (NSERC).

NOMENCLATURE

g	[m/s^2]	Gravitational acceleration
k	[W/mK]	Thermal conductivity
L	[m]	Length of heated plate
l	[m]	Mixing length
n	[-]	Constant
Nu	[-]	Nusselt number
Nu_{min}	[-]	Minimum Nusselt number value
Nu_{for}	[-]	Nusselt number in purely forced convection
Nu_{nat}	[-]	Nusselt number in purely natural convection
q'	[W/m^2]	Mean surface heat flux
$\dot{q}$	[W/m^2]	Uniform surface heat flux
Ra	[-]	Rayleigh number
Ra^*	[-]	Heat flux Rayleigh number
Re	[-]	Reynolds number
Re_{min}	[-]	Reynolds number at which minimum Nusselt number occurs
T	[K]	Temperature
T_f	[K]	Fluid temperature in undisturbed fluid
T_m	[K]	Mean plate surface temperature
U	[m/s]	Magnitude of forced velocity
$Wtop$	[-]	Dimensionless opening at top of blind
$Wbot$	[-]	Dimensionless opening at bottom of blind

Greek Symbols

α	[m^2/s]	Thermal diffusivity
β	[1/K]	Coefficient of thermal expansion
ν	[m^2/s]	Kinematic viscosity
ρ	[kg/m^3]	Density
φ	[^{o}]	Angle of inclination to the vertical
τ	[N/ m^2]	Viscous shear stress

REFERENCES

[1] Gryzagoridis J., Combined free and forced convection from an isothermal vertical plate, *International Journal of Heat and Mass Transfer*, Vol. 18, 1975, pp. 911-916.

[2] Babezha A.V., Gimbutis G.I., and Shvenchvanas P.P., Heat transfer at a vertical flat surface with the combined effect of forced and free convection in the same direction, *International Journal of Thermal Engineering*, Vol. 21, 1981, pp. 135-138.

[3] Carey V.P., and Gebhart B., Transport at large downstream distances in mixed convection flow adjacent to a vertical uniform-heat-flux surface, *International Journal of Heat and Mass Transfer,* Vol. 25(2), 1982, pp. 255-266.

[4] Churchill S.W., A comprehensive correlating equation for laminar, assisting, forced and free convection, *AIChE Journal* Vol. 23(1), 1977, pp. 10-16.

[5] Hall W.B., and Price P.H., Mixed forced and free convection from a vertical heated plate to air, *Proceedings of the 4th International Heat Transfer Conf.,* Vol. 4, Paper NC3.3, 1970.

[6] Oosthuizen P.H., and Bassey M., An experimental study of combined forced and free convection heat transfer from flat plates to air at low Reynolds numbers, *Transactions ASME, Series C, Journal of Heat Transfer,* Vol. 95(1),1973, pp. 120-121.

[7] Wilks G., Combined forced and free convection flow on vertical surfaces, *International Journal of Heat and Mass Transfer,* Vol. 16(10), 1973, pp. 1958-1964.

[8] Kitamura K., Yamamoto M., and Kimura F., Fluid flow and heat transfer of opposing mixed convection adjacent to vertical heated plates, *Heat Transfer. Asian Research*, Vol. 34(8), 2005, pp. 595-607.

[9] Merkin J.H., and Mahmood T., Mixed convection boundary layer similarity solutions: prescribed wall heat flux, *Zeitschrift für angewandte Mathematik und Physik* (Journal of Applied Mathematics and Physics-ZAMP), Vol. 40(1), 1989, pp. 51-68.

[10] Mucoglu A., and Chen T.S., Mixed convection on inclined surfaces, *Journal of Heat Transfer*, Vol. 101(3), 1979, pp. 422-426.

[11] Ramachandran N.N., Armaly B.F., and Chen T.S., Measurements of laminar mixed convection flow adjacent to an inclined surface, *Journal of Heat Transfer*, Vol. 109(1), 1987, pp. 146-150.

[12] Ramachandran N.N., Armaly B.F., and Chen T.S., Mixed convection over a horizontal plate, *Journal of Heat Transfer*, Vol. 105(2), 1983, pp. 420-423.

[13] Chen T.S., Sparrow E.M., and Mucoglu A.A., Mixed convection in boundary layer flow on a horizontal plate, *Journal of Heat Transfer*, Vol. 99(1), 1977, pp. 66-71.

[14] Chen T.S., Yuh C.F., and Moutsoglou A., Combined heat and mass transfer in mixed convection along vertical and inclined plates, *International Journal of Heat and Mass Transfer*, Vol. 23(4), 1980, pp. 527-537.

[15] Kitamura K., Matsumoto J., Mitsuishi A., and Misumi T., Fluid flow and heat transfer of opposing mixed convection adjacent to

downward-facing, inclined heated plates, *Heat Transfer. Asian Research*, Vol. 38(1), 2009, pp. 25-39.

[16] Wang X.A., An experimental study of mixed, forced, and free convection heat transfer from a horizontal flat plate to air, *Journal of Heat Transfer*, Vol. 104(1), 1982, pp. 139-144.

[17] Wickern G., Mixed convection from an arbitrarily inclined semi-infinite flat plate-I. The influence of the inclination angle, *International Journal of Heat and Mass Transfer*, Vol. 34(8), 1991, pp. 1935-1945.

[18] Wickern G., Mixed convection from an arbitrarily inclined semi-infinite flat plate-II. The influence of the Prandtl number, *International Journal of Heat and Mass Transfer*, Vol. 34(8), 1991, pp. 1947-1957.

[19] Chen T.S., Armaly B.F., and Ramachandran N.N., Correlations for laminar mixed convection flows on vertical, inclined, and horizontal flat plates, *Journal of Heat Transfer*, Vol. 108(4), 1986, pp.835-840.

[20] Abu-Mulaweh H.I., Chen T.S., and Armaly B.F., Effects of free-stream velocity on turbulent natural-convection flow along a vertical plate, *Experimental Heat Transfer*, 2000, Vol. 13, pp. 183-195.

[21] Abid C., Barberi Moine C., and Paini F., Application of the wavelet transform in e laminar turbulent transition for a flow in a mixed convection phenomenon, *The European Physical Journal B*, Vol. 13, 2000, pp. 707-714.

[22] Armaly B.F., Ramachandran N., and Chen T.S., 1986, Prediction of turbulent mixed convection along a vertical plate, *Proceedings of the 8th International Heat Transfer Conference,* Vol. 3, pp. 1445-1450.

[23] Behzadmehr A., Galanis N., and Laneville A., Laminar-turbulent transition for low Reynolds number mixed convection in a uniformly heated vertical tube, *International Journal of Numerical Methods for Heat and Fluid Flow*, Vol. 12(7), 2002, pp. 839-854.

[24] Cebeci T., Broniewski D., Joubert C., and Kural O., Mixed convection on a vertical flat plate with transition and separation, *Transactions ASME Journal of Heat Transfer*, Vol. 112, 1990, pp. 144-150.

[25] Chen T.S., Armaly B.F., and Ali M.M., Mixed convection in turbulent boundary layer flow along a vertical plate, *ASME Journal of Heat Transfer*, Vol. 109, 1987, pp. 251-253.

[26] Evans G., Greif R., Siebers D., and Tieszen S., Turbulent mixed convection from a large, high temperature, vertical flat surface, *International Journal of Heat and Fluid Flow*, Vol. 26, 2005, pp. 1-11.

[27] Krishnamurthy R., and Gebhart B., An experimental study of transition to turbulence in vertical mixed convection flows, *ASME Journal of Heat Transfer*, Vol. 111(1), 1989, pp. 121-130.

[28] Hattori Y., Tsuji T., Nagano Y., and Tanaka N., Characteristics of turbulent combined-convection boundary layer along a vertical heated plate, *International Journal of Heat and Fluid Flow*, Vol. 21, 2000, pp. 520-525.

[29] Hattori Y., Tsuji T., Nagano Y., and Tanaka N., Effects of freestream on turbulent combined combined-convection boundary layer along a vertical heated plate, *International Journal of Heat and Fluid Flow*, Vol. 22, 2001, pp. 315-322.

[30] Inagaki T., The criterion for turbulent combined forced and natural convection in a vertical flow system, *Transactions of the ASME Journal of Heat Transfer*, Vol. 118, 1996, pp. 213-215.

[31] Kitamura K., and Inagaki T., Turbulent heat and momentum transfer of combined forced and natural convection along a vertical flat plate-aiding flow, *International Journal of Heat and Mass Transfer*, Vol. 30(1), 1987, pp.23-41.

[32] Krishnamurthy R., and Gebhart B., Heat transfer by mixed convection in a vertical flow undergoing transition, *International Journal of Heat and Mass Transfer*, Vol. 29(8), 1986, pp.1211-1218.

[33] Venkatasubbaiah K., and Sengupta T.K., Mixed convection flow past a vertical plate: Stability analysis and its direct simulation, *International Journal of Thermal Sciences*, Vol. 48, 2009, pp. 461-474.

[34] Patel KK, Armaly B.F., and Chen T.S., Transition from turbulent natural to turbulent forced convection, *Journal of Heat Transfer*, Vol. 120(4), 1998, pp. 1086-1089.

[35] Abedina M.Z., Tsuji T., and Lee J., Turbulence characteristics and vortical structures in combined-convection boundary layers along a heated vertical flat plate, *International Journal of Heat and Mass Transfer*, Vol. 55(15-16), 2012, pp. 3995–4002.

[36] Jones W.P., and Launder B.E., The prediction of laminarization with a two-equation model of turbulence, *International Journal of Heat and Mass Transfer*, Vol. 15, 1973, pp. 301-314.

[37] Kenning D.R.B., Shock R.A.W., and Poon J.Y.M, Local reductions in heat transfer due to buoyancy effects in upward turbulent flow, *Proceedings of the 5th International Heat Transfer Conference,* Vol. 3, 1974, pp. 139-143

[38] Oosthuizen P.H., Turbulent combined convective flow over a vertical plane surface, *Proceedings of the 5th International Heat Transfer Conference,* Vol. 3, 1974, Paper NC4.1, pp. 129-133.

[39] Lee S.L., Chen T.S., Armaly B.F., Wave instability characteristics for the entire regime of mixed convection flow along vertical flat plates, *International Journal of Heat and Mass Transfer*, Vol. 30(8), 1987, pp. 1743-1751.

[40] Abu-Mulaweh H.I., Armaly B.F., and Chen T.S., Instabilities of mixed convection flows adjacent to inclined plates, *Journal of Heat Transfer*, Vol. 109(4), 1987, pp. 1031-1033.

[41] Lee S.L., Chen T.S., and Armaly B.F., Nonparallel wave instability of mixed convection flow on inclined flat plates, *International Journal of Heat and Mass Transfer*, Vol. 31(7), 1988, pp. 1385-1398.

[42] Moharreri S.S., Armaly B.F., and Chen T.S., Measurements in the transition vortex flow regime of mixed convection above a horizontal heated plate, *Journal of Heat Transfer*, Vol. 110(2), 1988, pp. 358-365.

[43] Tien H.C., Chen T.S., and Armaly B.F., Vortex instability of natural convection flow over horizontal and inclined plates with uniform surface heat flux, *Numerical Heat Transfer Part A-Applications*, Vol. 9(6), 1986, pp. 697-713.

[44] Mucoglu N., and Chen T.S., Wave instability of mixed convection flow along a vertical flat plate, *Numerical Heat Transfer,* Vol. 1, 1978, pp.267-283.

[45] Oosthuizen P.H., A numerical study of laminar and turbulent mixed convective flow over a vertical isothermal plate, *Proceedings of the 14th International Heat Transfer Conference*, Washington, Paper IHTC14-22448, 7-13 Aug., 2010.

[46] Oosthuizen P.H., and Paul J.T., A numerical study of laminar and turbulent mixed natural and forced convective flow over a vertical plate with a uniform surface heat flux, *Proceedings of the 18th CFD Annual Conference*, London, ON, 17-19 May, 2010.

[47] Oosthuizen P.H., A numerical study of laminar and turbulent opposing mixed convective flow over a vertical plate with a uniform surface heat flux, *Proceedings of the 10th International Conference on Heat Transfer, Fluid Mechanics and Thermodynamics* (HEFAT 2014), Orlando, 14-16 July, 2014.

[48] Oosthuizen P.H., Laminar and turbulent mixed convective heat transfer from an inclined isothermal plate, *Proceedings of the 21st Annual Conference of the CFD Society of Canada*, Sherbrooke, Paper 50, 6-9 May, 2013.

[49] Oosthuizen P.H., Laminar, transitional, and turbulent mixed convective heat transfer from a thin inclined plate having a uniform surface heat flux, *Proceedings of the 15th International Heat Transfer Conference*, Kyoto, Paper IHTC15-849710-15 Aug., 2014.

[50] Oosthuizen P.H., A numerical study of opposing mixed convective heat transfer from a vertical isothermal plate with laminar and turbulent flow, *Proceedings of the 11th AIAA/ASME Joint Thermophysics and Heat Transfer Conference*, Atlanta, AIAA-2014-2827, 16-20 June, 2014.

[51] Oosthuizen P.H., and Naylor D., *Introduction to Convective Heat Transfer Analysis*, 1st Edition, McGraw Hill, New York, 1999.

[52] Oosthuizen P.H., Numerical study of the effect of cold air vent flow on the convective heat transfer rate from a cold window covered by a top down-bottom up plane blind, *Proceedings of the ASME Summer Heat Transfer Conference*, Minneapolis, Paper HT2013-17165, 14-19 June, 2013.

[53] Oosthuizen P.H., and Naylor D., A numerical study of the effect of blind opening on laminar-to-turbulent transition in the flow over a Simple recessed window-plane blind system, *Proceedings of the ASME 2010 International Mechanical Congress & Exposition (IMECE 2010),* Vancouver, Paper IMECE2010-38175, 12-18 November, 2010.

[54] Plumb O.A., and Kennedy L.A., Application of a *k-e* turbulence model to natural convection from a vertical isothermal surface, *ASME Journal of Heat Transfer*, Vol. 99, 1977, pp 79-85.

[55] Schmidt R.C., and Patankar S.V., Simulating boundary layer transition with low Reynolds number *k-ε* turbulence models: Part 1- an evaluation of prediction characteristics, *Journal of Turbomachinery*, Vol. 113, 1991, pp 10-17.